

# Connecting NTK and NNGP: A Unified Theoretical Framework for Wide Neural Network Learning Dynamics

Yehonatan Avidan

*Racah Institute of Physics, The Hebrew University of Jerusalem, Jerusalem 91904, Israel and  
Edmond and Lily Safra Center for Brain Sciences, Hebrew University, Jerusalem 91904, Israel*

Qianyi Li

*The Biophysics Program, Harvard University, Cambridge, Massachusetts 02138, USA and  
Center for Brain Science, Harvard University, Cambridge, Massachusetts 02138, USA*

Haim Sompolinsky

*Racah Institute of Physics, The Hebrew University of Jerusalem, Jerusalem 91904, Israel  
Edmond and Lily Safra Center for Brain Sciences, Hebrew University, Jerusalem 91904, Israel and  
Center for Brain Science, Harvard University, Cambridge, Massachusetts 02138, USA*

(Dated: January 3, 2025)

Artificial neural networks have revolutionized machine learning in recent years, but a complete theoretical framework for their learning process is still lacking. Substantial theoretical advances have been achieved for wide networks, within two disparate theoretical frameworks: the Neural Tangent Kernel (NTK), which assumes linearized gradient descent dynamics, and the Bayesian Neural Network Gaussian Process (NNGP) framework. Here we unify these two theories using gradient descent learning dynamics with an additional small noise in an ensemble of wide deep networks. We construct an exact analytical theory for the network input-output function and introduce a new time-dependent Neural Dynamical Kernel (NDK) from which both NTK and NNGP kernels are derived. We identify two learning phases characterized by different time scales: an initial gradient-driven learning phase, dominated by deterministic minimization of the loss, in which the time scale is mainly governed by the variance of the weight initialization. It is followed by a slow diffusive learning stage, during which the network parameters sample the solution space, with a time constant that is determined by the noise level and the variance of the Bayesian prior. The two variance parameters can strongly affect the performance in the two regimes, particularly in sigmoidal neurons. In contrast to the exponential convergence of the mean predictor in the initial phase, the convergence to the final equilibrium is more complex and may exhibit nonmonotonic behavior. By characterizing the diffusive learning phase, our work sheds light on the phenomenon of representational drift in the brain, explaining how neural activity can exhibit continuous changes in internal representations without degrading performance, either by ongoing weak gradient signals that synchronize the drifts of different synapses or by architectural biases that generate invariant code, i.e., task-relevant information that is robust against the drift process. This work closes the gap between the NTK and NNGP theories, providing a comprehensive framework for understanding the learning process of deep wide neural networks and for analyzing learning dynamics in biological neural circuits.

## I. INTRODUCTION

Despite the empirical success of artificial neural networks, theoretical understanding of their underlying learning process is still limited. One promising theoretical approach focuses on deep wide networks, in which the number of parameters in each layer goes to infinity whereas the number of training examples remains finite [1–11]. In this regime, the neural network (NN) is highly over-parameterized, and there is a degenerate space of solutions achieving zero training error. Investigating the properties of the solution space offers an opportunity for understanding learning in over-parameterized NNs [12–14]. The two well-studied theoretical frameworks in the infinite width limit focus on two different scenarios for exploring the solution space during learning. One considers randomly initialized NNs trained with gradient descent

dynamics, and the learned NN parameters are largely dependent on their value at initialization. In this case, the infinitely wide NN’s input-output relation is captured by the Neural Tangent Kernel (NTK) [2, 4]. The other scenario considers Bayesian neural networks with an i.i.d. Gaussian prior over their parameters, and a learning-induced posterior distribution. In this case, the statistics of the NN’s input-output relation in the infinite width limit is given by the Neural Network Gaussian Process (NNGP) kernel [3, 15]. These two scenarios make different assumptions regarding the learning process and regularization. Furthermore, the generalization performance of the two kernels on benchmark datasets differs [16]. It is therefore important to generate a unified dynamical process with a single set of priors and regularizations that captures both cases. From a neuroscience perspective, a better understanding of the exploratory process leading

to Bayesian equilibrium may shed light on the empirical and hotly debated phenomenon of representational drift [17–23]. To this end, we derive a new analytical theory of the learning dynamics.

1. We derive analytical equations for the time evolution of the input-output relation (i.e. the predictor) of a network learning with Langevin gradient descent dynamics [24, 25]. We show that the equations for the mean and variance of the predictor are in the form of integral equations, and present their numerical solutions for benchmark datasets.

2. A new time-dependent kernel, the Neural Dynamical Kernel (NDK), naturally emerges from our theory. This kernel can be understood as a time-dependent generalization of the known NTK.

3. Our theory reveals two important learning phases characterized by different time scales: gradient-driven, and diffusive learning. In the initial gradient-driven learning phase, the dynamics are primarily governed by deterministic gradient descent and described by the NTK theory. This phase is followed by the slow exploration stage, during which the network parameters sample the solution space, ultimately approaching the equilibrium posterior distribution corresponding to NNGP (Another perspective on the two phases was offered in [26, 27]).

4. We show that the generalization error may exhibit diverse behaviors during the diffusive learning phase depending on the network activation function, initialization, and regularization strength. Our theory provides insights into the roles of these hyper-parameters in the trajectory of the dynamics.

5. Through analysis of the temporal correlation between network weights during diffusive learning, we show that despite the random diffusion of hidden layer weights, the training error remains low due to learning signal causing continuous realignment of the readout and the hidden layer weights. Conversely, ceasing this signal decreases the network performance due to decorrelation of the representations, ultimately leading to degraded generalization. We derive conditions under which the performance upon completely decorrelated readout and hidden weights remains well above chance. This provides insight into potential mechanisms for maintaining cognitive computation in the presence of representational drift, which can be tested in biological neural circuits.

## II. MODEL

In this section, we describe the learning dynamics of fully connected Deep Neural Networks (DNNs) using Langevin dynamics. We first define the model and our notations.

### A. Notations and Setup for the Dynamical Theory

We consider a fully connected DNN with an input  $\mathbf{x} \in \mathbb{R}^{N_0}$ ,  $L$  hidden layers, and a single output  $f(\Theta, \mathbf{x})$  (i.e. the predictor), where  $\Theta$  denotes all weight parameters. The input-output function is given by:

$$f(\Theta, \mathbf{x}) = \frac{1}{\sqrt{N_L}} \mathbf{a} \cdot \mathbf{x}^L, \quad \mathbf{a} \in \mathbb{R}^{N_L} \quad (1)$$

$$\mathbf{x}^l(\mathbf{x}) = \phi(\mathbf{z}^l(\mathbf{x})), \quad \mathbf{z}^l \in \mathbb{R}^{N_l}, \quad l = 1, \dots, L \quad (2)$$

where the preactivations  $\mathbf{z}^l(\mathbf{x})$  are defined as

$$\mathbf{z}^l(\mathbf{x}) = \frac{1}{\sqrt{N_{l-1}}} \mathbf{W}^l \cdot \mathbf{x}^{l-1}(\mathbf{x}) \quad (3)$$

$N_l$  denotes the number of nodes in hidden layer  $l$ , and  $N_0$  is the input dimension.  $\mathbf{a} \in \mathbb{R}^{N_L}$  denotes the linear readout weights and  $\mathbf{W}^l \in \mathbb{R}^{N_l \times N_{l-1}}$  denote the hidden layer weights between layers  $l-1$  and  $l$ .  $\phi(\mathbf{z})$  is an element-wise nonlinear function of the preactivation vector. The set of all hidden layer weights is denoted as  $\mathbf{W} \equiv \{\mathbf{W}^1, \dots, \mathbf{W}^L\}$  and all the network parameters are denoted collectively as  $\Theta \equiv \{\mathbf{W}, \mathbf{a}\}$ .  $\mathbf{x}^l$  stands for the activations of the neurons in the  $l$ -th layer, and  $\mathbf{x} \in \mathbb{R}^{N_0}$  represents the input vector to the first layer of the network ( $\mathbf{x}^{l=0} \equiv \mathbf{x}$ ). The training data is a set of  $P$  labeled examples  $\mathcal{D} : \{\mathbf{x}^\mu, y^\mu\}_{\mu=1, \dots, P}$  where  $\mathbf{x}^\mu \in \mathbb{R}^{N_0}$  is a training data point, and  $y^\mu \in \mathbb{R}$  is the target label of  $\mathbf{x}^\mu$ . It is convenient to define a vector that contains all the label values  $Y \in \mathbb{R}^P$  and a vector of the predictor values on all the training points  $f_{\text{train}}(t) \in \mathbb{R}^P$ , such that  $f_{\text{train}}^\mu = f(\Theta, \mathbf{x}^\mu)$ .

We assume an architecture with a single output unit for the ease of notation. It is straightforward to generalize the model and our theory to multiple outputs, (see SI Sec. D).

We consider the following supervised learning cost function:

$$E(\Theta_t | \mathcal{D}) = \frac{1}{2} \sum_{\mu=1}^P (f_{\text{train}}^\mu(t) - y^\mu)^2 + \frac{T}{2\sigma^2} |\Theta_t|^2 \quad (4)$$

The first term is the loss function, specifically square error empirical loss (SE loss), and the second term is a regularization term that favors weights with small  $L_2$  norm (weight decay term).  $L_2$  regularization term has been shown to improve the generalization performance [28, 29]. We introduce the parameter  $T\sigma^{-2}$  as controlling the relative strength of the regularization and the SE loss. The reason for using both temperature  $T$  and  $\sigma$  is that the temperature  $T$  separately controls the level of noise in the stochastic dynamics (as will be defined below), and  $\sigma^2$  is equivalent to the variance of the Gaussian prior in a Bayesian framework.

We consider gradient descent learning dynamics with an additive noise given by continuous-time Langevin

equation. The weights of the system start from an i.i.d. Gaussian initial condition with zero mean and variance  $\sigma_0^2$ . The weights evolve under gradient descent with respect to the cost function above with noise  $\xi$ :

$$\frac{d}{dt}\Theta_t = -\nabla_{\Theta}E(\Theta_t) + \xi(t) \quad (5)$$

where  $\xi(t)$  has a white noise statistics  $\langle \xi(t) \rangle = 0$ ,  $\langle \xi(t)\xi^\top(t') \rangle = 2IT\delta(t-t')$ . The temperature  $T$  controls the level of noise in the system. We note that during the learning dynamics defined above, the dataset  $\mathcal{D}$  and inputs  $\mathbf{x}$  are constant in time. Hence, the time dependence of the predictor  $f$  is through the dynamics of the weight parameters, i.e.  $f(t, \mathbf{x}) \equiv f(\Theta_t, \mathbf{x})$ . Likewise,  $\mathbf{x}_t^l(\mathbf{x}) = \mathbf{x}^l(\mathbf{W}_t, \mathbf{x})$  and  $\mathbf{z}_t^l(\mathbf{x}) = \mathbf{z}^l(\mathbf{W}_t, \mathbf{x})$ .

Given a distribution of initial weights, the Langevin dynamics defines a time-dependent posterior distribution on weight space,  $P_t(\Theta)$ , which converges at long times to an equilibrium Gibbs distribution,  $P_{eq}(\Theta) \propto \exp(-\frac{1}{T}E(\Theta))$ . This distribution is equivalent to the posterior of the Bayesian formulation of learning [30].

**The Dynamics of the Prior:** In the absence of training signal the Langevin dynamics are a random walk with a quadratic potential (An Ornstein-Uhlenbeck process [31]). The induced statistics of  $\Theta$  is that of temporally correlated i.i.d Gaussian variables with zero mean

$$\langle \Theta_t \rangle_0 = 0, \quad \langle \Theta_t \Theta_{t'}^\top \rangle_0 = m(t, t')I \quad (6)$$

$$m(t, t') = \sigma^2 e^{-T\sigma^{-2}|t-t'|} + (\sigma_0^2 - \sigma^2) e^{-T\sigma^{-2}(t+t')} \quad (7)$$

Where  $\langle \cdot \rangle_0$  denotes henceforth averaging over the dynamics induced by the regularization and the noise. As expected,  $m(0,0) = \sigma_0^2$ . At long times, the second term of Eq.7 representing the transient of the dynamics vanishes and the dominant term is  $\sigma^2 e^{-T\sigma^{-2}|t-t'|}$ , with no dependence on  $\sigma_0^2$ .

### B. Two Phases of Learning in the Limit of Small Noise

We focus on the dynamics of overparameterized DNNs in the limit of small noise -  $T \rightarrow 0$ . Overparameterization creates a degeneracy, where many sets of parameters  $\Theta$  achieve a zero loss function, defining the solution space to the optimization problem. While these states are equivalent in performance on the training data, they differ in performance on unseen test examples. At low  $T$  the Gibbs distribution facilitates generalization by sampling the solution space with  $L_2$  bias.

In the small noise limit, a separation of time scales emerges due to the scales of the different components of the dynamics. During the initial gradient-driven phase, the loss is  $\mathcal{O}(1)$ , while the regularization term and the noise are  $\mathcal{O}(T)$ . Thus, when the temperature is low,

the loss dominates the dynamics, making them approximately deterministic. After a time of  $\mathcal{O}(1)$ , the network reaches a low training error solution where the loss function is  $\mathcal{O}(T)$ . At this stage, the residual loss signal is of the same order as the noise and regularization terms, leading to richer dynamics as the solution space is explored. These dynamics involve all three components and are no longer deterministic. As we show below, even in the infinite-width limit, these dynamics are not simple exponential relaxation. We emphasize that even though during the diffusive dynamics the fluctuations in training error remain  $\mathcal{O}(T)$  (see Fig.1 (b)). The weights themselves undergo a constrained random walk in the solution subspace (see Fig.1 (c)), with fluctuations of the scale of  $\sigma$ . The test performance also exhibits large fluctuations of the same order (Fig.1 (a)). At the end of the diffusive learning phase, the network reaches an equilibrium state where the overall statistics of the weight no longer change, converging to a Gibbs distribution.

### III. MOMENT GENERATING FUNCTION OF THE PREDICTOR IN THE LARGE WIDTH LIMIT

The performance of the network is determined by its input-output function, hence we are mainly interested in the predictor statistics induced by the Langevin dynamics at all times. SI Sec.B presents a derivation of a path-integral formulation of the above Langevin dynamics using a Markov proximal learning framework.

Evaluating statistical quantities using these integrals is generally intractable. However, in the infinite width limit, where the hidden layer widths are taken to infinity, i.e.  $N_0, \dots, N_L \rightarrow \infty$ , while the number of training examples  $P$  remains finite, the moments of the predictor can be derived from a moment generating function (MGF) formulation

$$\mathcal{M}[\ell] \equiv \left\langle \exp \left( \sum_{\mathbf{x}} \int dt \ell(t, \mathbf{x}) f(t, \mathbf{x}) \right) \right\rangle_{\Theta} \quad (8)$$

$$\langle f^n(t, \mathbf{x}) \rangle_{\Theta} = \left. \frac{\partial^n \mathcal{M}[\ell]}{\partial \ell^n(t, \mathbf{x})} \right|_{\ell(t, \mathbf{x})=0} \quad (9)$$

The square brackets  $[\cdot]$  represent a functional of the argument and the angular brackets denote the average of the statistics of all the possible trajectories of the weight parameters, marginalizing over the noise and the random initial condition.  $\ell(t, \mathbf{x})$  is the source term of the MGF, and taking derivatives w.r.t. the source yields the statistics of the predictor at time  $t$  on an input  $\mathbf{x}$ . In the infinite width limit,  $\mathcal{M}[\ell]$  takes the form of a path integral over two time-dependent vectors,  $f_{\text{train}}(t) \in \mathbb{R}^P$  and  $u(t) \in \mathbb{R}^P$ .  $f_{\text{train}}(t)$  was introduced before, and is the vector gathering the predictor values on the training examples, while  $u(t)$  is an auxiliary field which mediates the interactions between  $f_{\text{train}}(t)$  at different times.

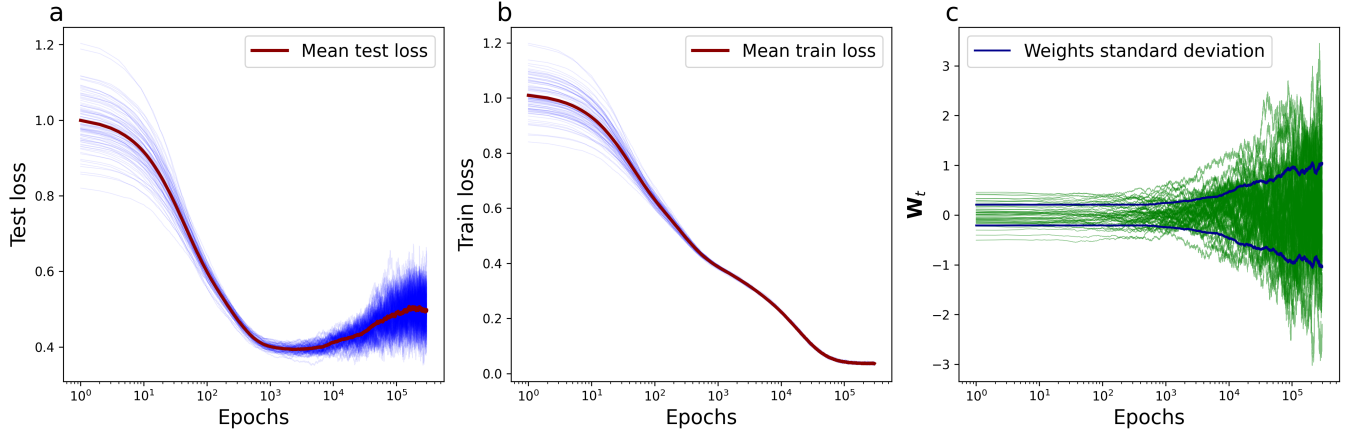


FIG. 1. Two Phases of Learning Dynamics: Simulation results of a deep network with a single hidden layer and error function activation, trained by Langevin dynamics (Eq.5) on binary classification using two classes from CIFAR-10 dataset [32]. (a) Test loss: The mean squared error (MSE) loss on test data reveals two distinct phases: an initial fast, approximately deterministic stage culminating in convergence to a low error and a subsequent slow, stochastic exploration phase characterized by large fluctuations. At long times, the network converges to an equilibrium state where the statistics of the weights and performance stabilize over time. (b) Training loss: The loss on the training data shows rapid relaxation to a state with low training error, with fluctuations on the order of  $\mathcal{O}(T)$ , indicating the restricted diffusive dynamics in the subspace of low training error. (c) Weight dynamics: The weights exhibit a constrained random walk process, with their standard deviation gradually increasing from an initial value  $\sigma_0$  to the equilibrium value  $\sigma$  (in this example  $\sigma > \sigma_0$ ). This stochastic process remains confined to the solutions subspace as evident by the low training error (b). Parameter and details are in Sec. H.

$$\mathcal{M}[\ell] = \int Df_{\text{train}} \int Du \exp(-S[f_{\text{train}}, u] - Q[\ell, f_{\text{train}}, u]) \quad (10)$$

$$S[f_{\text{train}}, u] = \frac{1}{2} \int_0^\infty dt \int_0^\infty dt' m(t, t') u^\top(t) K^L(t, t') u(t') \quad (11)$$

$$+ i \int_0^\infty dt \left( \int_0^t dt' [K_d^L(t, t') (Y - f_{\text{train}}(t'))] - f_{\text{train}}(t) \right)^\top u(t)$$

$$Q[\ell, f_{\text{train}}, u] = - \sum_{\mathbf{x}} \int_0^\infty dt \int_0^t dt' (k_d^L(t, t', \mathbf{x}))^\top (Y - f_{\text{train}}(t)) \ell(t, \mathbf{x}) \quad (12)$$

$$+ i \sum_{\mathbf{x}} \int_0^\infty dt \int_0^\infty dt' m(t, t') (k^L(t, t', \mathbf{x}))^\top u(t') \ell(t, \mathbf{x})$$

$$- \frac{1}{2} \sum_{\mathbf{x}, \mathbf{x}'} \int_0^\infty dt \int_0^\infty dt' m(t, t') \mathcal{K}^L(t, t', \mathbf{x}, \mathbf{x}') \ell(t, \mathbf{x}) \ell(t', \mathbf{x}')$$

Where  $Df_{\text{train}}, Du$  stands for a summation over all possible trajectories of the time-dependent vectors  $f_{\text{train}}(t), u(t)$ . Thus, the MGF defines a Gaussian measure on  $f_{\text{train}}(t)$  and  $u(t)$ .  $S[f_{\text{train}}, u]$  is a functional represents the source-independent part and is related to the dynamics of the predictor on the training data,

while  $Q[\ell, f_{\text{train}}, u]$  is a functional contains the source-dependent part and determines the dynamics of the predictor on a test point. The scalar coefficient  $m(t, t')$  is the time-dependent auto-correlations of the weights w.r.t. the Gaussian prior, Eqs. 6-7. The remaining coefficients of the MGF are various two-time kernel functions

defined in the next section.

#### IV. THE NEURAL DYNAMICAL KERNEL

We introduce the definitions of the kernels appearing in Eq.10, and the relations between these kernels and the known NTK [2] and NNGP [3] kernels. The quantity  $K^L(t, t')$  appearing in Eq.10 is a  $P \times P$  matrix  $K_{\mu\nu}^L(t, t') = \mathcal{K}^L(t, t', \mathbf{x}_\mu, \mathbf{x}_\nu)$  where  $(\mathbf{x}_\mu, \mathbf{x}_\nu)$  are a pair of training input vectors and  $\mathcal{K}^l(t, t', \mathbf{x}, \mathbf{x}')$  is a kernel function, defined for any two inputs  $\mathbf{x}, \mathbf{x}'$  and any layer  $l$  as

$$\mathcal{K}^l(t, t', \mathbf{x}, \mathbf{x}') = \frac{1}{N_l} \langle \mathbf{x}_t^l(\mathbf{x}) \cdot \mathbf{x}_{t'}^l(\mathbf{x}') \rangle_0 \quad (13)$$

The integer  $N_l$  is the width of the  $l$ -th layer and the average is w.r.t. to the prior statistics (Eq.6). At equal times  $t = t'$ , the kernel function is equivalent to the usual NNGP kernel function, as the average is over Gaussian parameters with time-dependent variance  $\mathcal{N} \sim (0, m(t, t))$  (see Eq.7) which transitions between  $\sigma_0^2$  at initialization to  $\sigma^2$  at long times.

The quantity  $K_d^L(t, t')$  appearing in Eq.10, is also a  $P \times P$  matrix,  $K_{d,\mu\nu}^L(t, t') = \mathcal{K}_d^L(t, t', \mathbf{x}_\mu, \mathbf{x}_\nu)$  where  $(\mathbf{x}_\mu, \mathbf{x}_\nu)$  are a pair of training input vectors. This matrix is defined via a novel Neural Dynamical Kernel (NDK) function of any two input vectors, as follows

$$\mathcal{K}_d^L(t, t', \mathbf{x}, \mathbf{x}') = e^{-T\sigma^{-2}|t-t'|} \langle \nabla_{\Theta} f(t, \mathbf{x}) \cdot \nabla_{\Theta} f(t', \mathbf{x}') \rangle_0 \quad (14)$$

where  $\nabla_{\Theta} f(t, \mathbf{x}) \equiv \nabla_{\Theta} f(\Theta, \mathbf{x})|_{\Theta_t}$  where  $\Theta_t$  obeys the stochastic statistics given in Eqs.6-7. At equal times:  $t = t'$ , this kernel has a simple relation to the NTK [2]. Specifically,

$$\mathcal{K}_d^L(t = t', \mathbf{x}, \mathbf{x}') = K_{NTK}^L(\mathbf{x}, \mathbf{x}')_{\mathcal{N} \sim (0, m(t, t))} \quad (15)$$

In particular, at initialization -  $\mathcal{K}_d^L(t = 0, t' = 0, \mathbf{x}, \mathbf{x}') = \mathcal{K}_{NTK}^L(\mathbf{x}, \mathbf{x}')$ , where the average is only on the weights random initial condition, like in the usual NTK. Furthermore, the NNGP kernel can also be evaluated from the NDK by an integral over long times (see SI Sec.E for detailed proof)

$$\lim_{t \rightarrow \infty} \left( \frac{T}{\sigma^2} \int_0^t \mathcal{K}_d^L(t, t', \mathbf{x}, \mathbf{x}') dt' \right) = \mathcal{K}_{GP}^L(\mathbf{x}, \mathbf{x}') \quad (16)$$

Where  $\mathcal{K}_{GP}^L(\mathbf{x}, \mathbf{x}') = \frac{1}{N_l} \langle \mathbf{x}^l(\mathbf{x}) \cdot \mathbf{x}^l(\mathbf{x}') \rangle_{\mathcal{N} \sim (0, \sigma^2)}$ . This identity is important for reaching the Bayesian equilibrium at long times (see Sec.VB) and is related to the well-known relation between correlations and response functions, the Fluctuation Dissipation Theorem (FDT)

in statistical mechanics [33]. The NDK can be obtained recursively in terms of the time-dependent kernel  $\mathcal{K}^l(t, t', \mathbf{x}, \mathbf{x}')$  and the derivative kernel  $\dot{\mathcal{K}}^l(t, t', \mathbf{x}, \mathbf{x}')$ , similarly to the NTK (see SI Sec.E for detailed proof).

$$\begin{aligned} \mathcal{K}_d^L(t, t', \mathbf{x}, \mathbf{x}') = & \\ m(t, t') \dot{\mathcal{K}}^L(t, t', \mathbf{x}, \mathbf{x}') \mathcal{K}_d^{L-1}(t, t', \mathbf{x}, \mathbf{x}') & \\ + e^{-T\sigma^{-2}|t-t'|} \mathcal{K}^L(t, t', \mathbf{x}, \mathbf{x}') & \end{aligned} \quad (17)$$

$$\mathcal{K}_d^{l=0}(t, t', \mathbf{x}, \mathbf{x}') = e^{-T\sigma^{-2}|t-t'|} \left( \frac{1}{N_0} \mathbf{x} \cdot \mathbf{x}' \right) \quad (18)$$

The derivative kernel,  $\dot{\mathcal{K}}^l(t, t', \mathbf{x}, \mathbf{x}')$  appearing in Eq.17 is the dot product of the derivative of the activation function

$$\dot{\mathcal{K}}^l(t, t', \mathbf{x}, \mathbf{x}') = \frac{1}{N_l} \langle \phi'(\mathbf{z}_t^l(\mathbf{x})) \cdot \phi'(\mathbf{z}_{t'}^l(\mathbf{x}')) \rangle_0 \quad (19)$$

Where  $\phi'$  stands for elementwise derivative of the activation of the layer  $l$  w.r.t to their preactivations  $(\frac{\partial \phi(\mathbf{z})}{\partial \mathbf{z}})$ , induced by a given input at time  $t$ . The time-dependent kernels  $\mathcal{K}^L$  and  $\dot{\mathcal{K}}^L$  obey recursion relations similar to their static counterparts (see SI Sec.E). These recursion relations - as well as those of Eq.17 - have a closed-form expression for some nonlinearities such as ReLU and error function (inspired by the static expressions for these kernels [10, 15]), and explicit solutions for linear activation (see SI Sec.E). Finally, in Eqs.11,12,  $k_\mu^L(t, t', \mathbf{x}) \in \mathbb{R}^{P \times 1}$  and  $k_d^L(t, t', \mathbf{x}) \in \mathbb{R}^{P \times 1}$  are vectors of the kernels of a test point with the training data, such that  $k_\mu^L(t, t', \mathbf{x}) = \mathcal{K}^L(t, t', \mathbf{x}, \mathbf{x}_\mu)$ , and similarly  $k_{d,\mu}^L(t, t', \mathbf{x}) = \mathcal{K}_d^L(t, t', \mathbf{x}, \mathbf{x}_\mu)$ . For the convenience of the reader we summarize all the relevant kernel functions in the following table:

Name	Notation	Definition
NNGP kernel	$\mathcal{K}_{GP}^L(\mathbf{x}, \mathbf{x}')$	$(N_l)^{-1} \langle \phi(\mathbf{z}^l(\mathbf{x})) \cdot \phi(\mathbf{z}^l(\mathbf{x}')) \rangle_{\mathcal{N} \sim (0, \sigma^2)}$
NTK	$\mathcal{K}_{NTK}^L(\mathbf{x}, \mathbf{x}')$	$\langle \nabla_{\Theta} f(t = 0, \mathbf{x}) \cdot \nabla_{\Theta} f(t' = 0, \mathbf{x}') \rangle_{\mathcal{N} \sim (0, \sigma_0^2)}$
NDK	$\mathcal{K}_d^L(t, t', \mathbf{x}, \mathbf{x}')$	$e^{-T\sigma^{-2} t-t' } \langle \nabla_{\Theta} f(t, \mathbf{x}) \cdot \nabla_{\Theta} f(t', \mathbf{x}') \rangle_0$
Time-dependent kernel	$\mathcal{K}^l(t, t', \mathbf{x}, \mathbf{x}')$	$(N_l)^{-1} \langle \phi(\mathbf{z}_t^l(\mathbf{x})) \cdot \phi(\mathbf{z}_{t'}^l(\mathbf{x}')) \rangle_0$
Time-dependent derivative kernel	$\dot{\mathcal{K}}^l(t, t', \mathbf{x}, \mathbf{x}')$	$(N_l)^{-1} \langle \phi'(\mathbf{z}_t^l(\mathbf{x})) \cdot \phi'(\mathbf{z}_{t'}^l(\mathbf{x}')) \rangle_0$

**ReLU Dynamical Kernel:** Due to its homogeneity property, i.e.  $\text{ReLU}(\lambda x) = \lambda \cdot \text{ReLU}(x)$ , altering the variance of the weight distribution changes the global scale of the kernel but does not change its structural properties. This implies that the equal-time kernel in ReLU preserves its structure, encoding the underlying data correlations (see Fig. 2 (a-c)).

We analyze the effect of time differences on the ReLU NDK. The ReLU kernel depends on the angle between two inputs, defined as  $\theta(\mathbf{x}, \mathbf{x}') = \frac{\mathbf{x} \cdot \mathbf{x}'}{\|\mathbf{x}\| \|\mathbf{x}'\|}$ . When the time difference is large, the inputs become uncorrelated due to

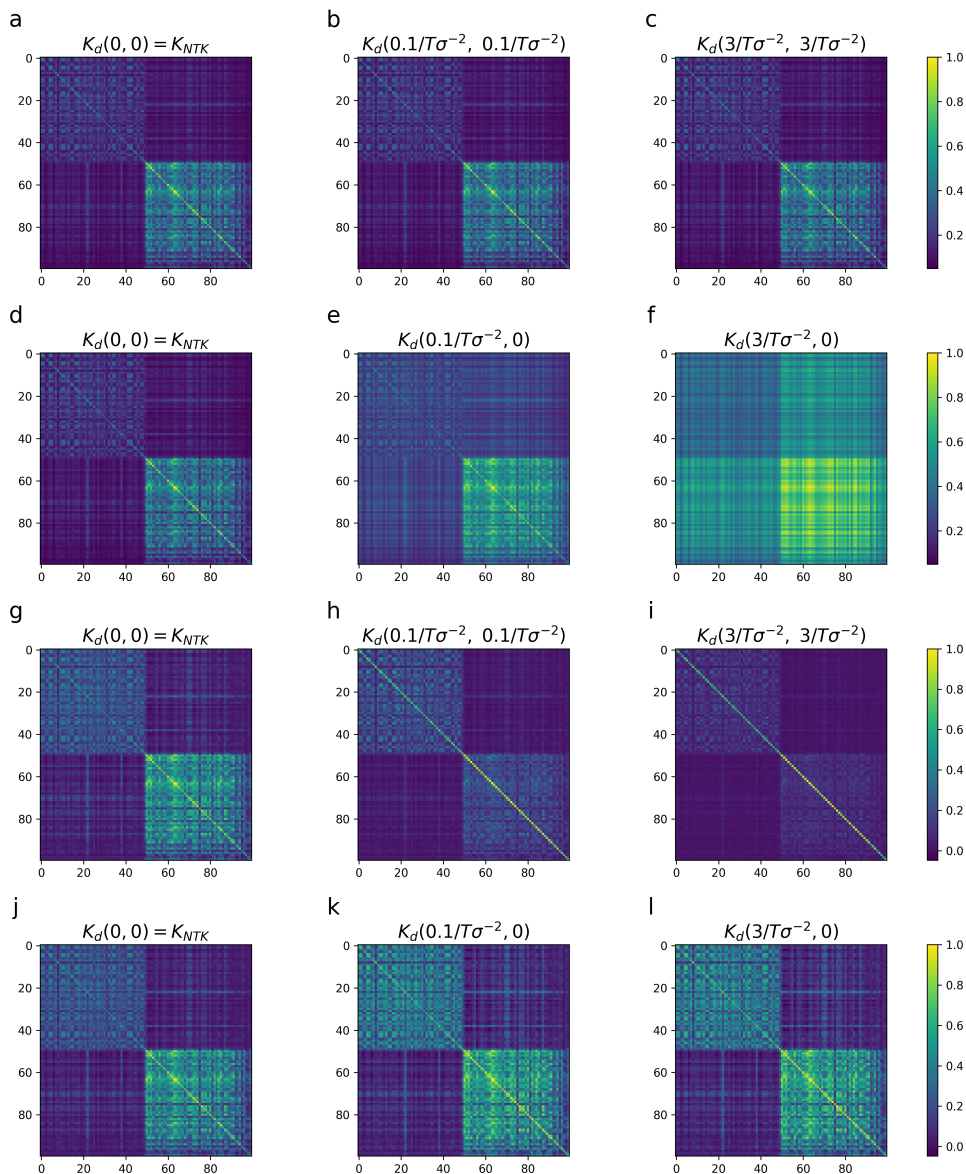


FIG. 2. The Neural Dynamical Kernel (NDK): The figure presents the NDK for various nonlinearities, parameters, and times, using examples from the MNIST dataset (0,1 digits). To focus on the kernel's structure independently of scale, the kernels are normalized by their maximum value. We present the NDK for equal times ( $t = t'$ , Eq.15) and for time difference from initialization (evaluating Eq.17 at  $t' = 0$ ) (a-c) ReLU kernel (equal times) with parameters  $\sigma_0 = 0.2$  and  $\sigma = 1$ . Since ReLU is a homogeneous function, changes in the variance of the distribution do not alter the kernel's structure, which is preserved for all times. (d-f) ReLU kernel (time difference): The ReLU kernel depends on the angles between pairs of input vectors. As the time difference increases, the representations decouple, leaving only information about the amplitude of each example,  $\|\mathbf{x}_\mu\|$ , which is reflected in the rows and columns of the kernel. This uncorrelated kernel is critical for understanding representational drift (see Sec.VII) (g-i) Error Function kernel (equal times) with parameters  $\sigma_0 = 0.2$  and  $\sigma = 10$ . For small  $\sigma_0$ , the kernel resembles a linear kernel, closely reflecting the structure of the input. A large  $\sigma$  causes a step-function-like behavior of the kernel, with a strong peak along the diagonal. (j-l) Error Function kernel (time difference) with parameters  $\sigma_0 = 0.2$  and  $\sigma = 10$ . The effect of time difference is similar to that of small variance, resulting in a kernel that resembles a linear kernel.

random fluctuations in the weights. As a result, all angles between different inputs approach  $\theta_{\mu\nu} \rightarrow (1 - \delta_{\mu\nu}) \frac{\pi}{2}$ , leading to a loss of structure in the kernel (see Fig. 2 (d-f)). In this scenario, the only information retained is the

amplitudes of the inputs,  $\|\mathbf{x}\|$  and  $\|\mathbf{x}'\|$ . This behavior is critical for understanding representational drift, as we discuss in Sec.VII.

**Sigmoidal Dynamical Kernel:** Sigmoidal functions

are defined as monotonically increasing functions with linear behavior around zero and saturation at both  $\pm\infty$ . Examples of such functions include hyperbolic tangent and error function. These functions are sensitive to changes in the variance of the weights. When the variance is small, the kernel closely resembles a linear kernel. On the other hand, when the variance is large, the function acts like a step function, leading to strong non-linearity. In the NDK, this nonlinearity is most prominent along the diagonal due to the influence of the derivative kernel, as shown in Fig. 2 (g-i).

In sigmoidal functions, significant time differences result in a kernel that is nearly linear. Unlike the ReLU kernel, the structure of the kernel is preserved, with the primary effect being a change in its scale (see Fig.2(j-l)).

**The Mean Predictor:** The above explicit expression for the MGF allows for the evaluation of the statistics of the predictor by differentiating the MGF w.r.t. to the source  $\ell(t, \mathbf{x})$ . The equations describing the second moment for a general nonlinearity are complex, and given in SI Sec.C. Here we bring the equations for the mean predictor for train and test.

The mean predictor on the training inputs obeys the following integral equation

$$\langle f_{\text{train}}(t) \rangle = \int_0^t dt' K_d^L(t, t') (Y - \langle f_{\text{train}}(t') \rangle) \quad (20)$$

where the average on  $\langle f_{\text{train}}(t) \rangle$  is over all possible trajectories of the parameters, encompassing both the randomness of the noise and the initial condition. The mean predictor on any test point  $\mathbf{x}$  is given by an integral over the training predictor with the NDK of the test

$$\langle f(t, \mathbf{x}) \rangle = \int_0^t dt' k_d^L(t, t', \mathbf{x})^\top (Y - \langle f_{\text{train}}(t') \rangle) \quad (21)$$

## V. DYNAMICS AT LOW $T$

As discussed in Sec.IIB, in the limit of  $T \rightarrow 0$ , the learning dynamics can be divided into two distinct phases: a gradient-driven phase, occurring on a timescale of  $\mathcal{O}(1)$  and dominated by deterministic minimization of the SE loss, and a diffusive phase, during which the weights explore the solution subspace, and characterized by time scale of  $t \sim \mathcal{O}(1/T)$ .

### A. Gradient-Driven Phase Corresponds to NTK Dynamics

The time dependence of the NDK (Eq.17) comes from exponents with time scale of  $\sigma^2/T$  (Eqs.7, 17), and thus, in the limit of  $T \rightarrow 0$  and  $t \sim \mathcal{O}(1)$ , we can substitute  $\mathcal{K}_d^L(t, t', \mathbf{x}, \mathbf{x}') = \mathcal{K}_d^L(t=0, t'=0, \mathbf{x}, \mathbf{x}') = \mathcal{K}_{NTK}^L(\mathbf{x}, \mathbf{x}')$  in Eq. 20.

**Mean predictor:** Differentiating Eq.20 reduces the integral equation into the following linear ODE

$$\begin{aligned} \frac{d}{dt} \langle f_{\text{train}}(t) \rangle &= K_{NTK}^L (Y - \langle f_{\text{train}}(t) \rangle) \\ \langle f_{\text{train}}(t=0) \rangle &= 0 \end{aligned} \quad (22)$$

Which yields  $\lim_{T \rightarrow 0} \langle f_{\text{train}}(t) \rangle = (I - \exp(-K_{NTK}^L t)) Y$ , and the well-known mean predictor in the NTK theory [2]:

$$\begin{aligned} \lim_{T \rightarrow 0} \langle f(t, \mathbf{x}) \rangle &= \\ k_{NTK}^L(\mathbf{x})^\top (K_{NTK}^L)^{-1} (I - \exp(-K_{NTK}^L t)) Y \end{aligned} \quad (23)$$

We define  $K_{NTK}^L \in \mathbb{R}^{P \times P}$  and  $k_{NTK}^L(\mathbf{x}) \in \mathbb{R}^P$  as the NTK applied on the train and test data respectively, similarly to Sec.IV.

In this regime both the Langevin noise and the  $L_2$  regularizer can be neglected, resulting in dynamics that can be approximated by gradient descent, as assumed in the NTK theory. In particular, the ‘‘NTK equilibrium’’ defined by first taking  $T \rightarrow 0$  and then  $t \rightarrow \infty$ , yields the well-known static NTK result

$$\lim_{t \rightarrow \infty} \lim_{T \rightarrow 0} \langle f(t, \mathbf{x}) \rangle = k_{NTK}^L(\mathbf{x})^\top (K_{NTK}^L)^{-1} Y \quad (24)$$

The NTK equilibrium signifies the transition between the gradient-driven phase and the diffusive learning phase, after which the effect of the Langevin noise and the  $L_2$  regularizer cannot be neglected.

**Predictor covariance:** We present the results of the covariance of the predictor in the NTK theory, achieved by taking the limit  $T \rightarrow 0$  of the expressions of the second moment in our theory (see SI Sec.C for details). For the predictor of training points

$$\begin{aligned} \lim_{T \rightarrow 0} \sigma_0^{-2} \langle \delta f_{\text{train}}(t) \delta f_{\text{train}}^\top(t') \rangle &= \\ \exp(-K_{NTK}^L t) K_{GP_0}^L \exp(-K_{NTK}^L t') \end{aligned} \quad (25)$$

We denote  $K_{GP_0}$  as  $K_{GP}^L(\sigma = \sigma_0)$ , where the statistics of the kernel are over the Gaussian initialization with  $\sigma_0$  standard deviation, and not the Gaussian prior. The variance on the training data vanishes at long times, as all the outputs converge to their target labels. The covariance of the test inputs is

$$\begin{aligned} \lim_{T \rightarrow 0} \sigma_0^{-2} \langle \delta f(t, \mathbf{x}) \delta f(t', \mathbf{x}') \rangle &= \mathcal{K}_{GP_0}^L(\mathbf{x}, \mathbf{x}') - k_{GP_0}^L(\mathbf{x}) (K_{GP_0}^L)^{-1} k_{GP_0}^L(\mathbf{x}') \\ &+ \left[ (I - \exp(-K_{NTK}^L t)) (K_{NTK}^L)^{-1} k_{NTK}^L(\mathbf{x}) - (K_{GP_0}^L)^{-1} k_{GP_0}^L(\mathbf{x}) \right]^\top K_{GP_0}^L \\ &\cdot \left[ (I - \exp(-K_{NTK}^L t')) (K_{NTK}^L)^{-1} k_{NTK}^L(\mathbf{x}') - (K_{GP_0}^L)^{-1} k_{GP_0}^L(\mathbf{x}') \right] \end{aligned} \quad (26)$$

Taking the limit of  $t, t' \rightarrow \infty$  yields

$$\begin{aligned} \lim_{t, t' \rightarrow \infty} \lim_{T \rightarrow 0} \sigma_0^{-2} \langle \delta f(t, \mathbf{x}) \delta f(t', \mathbf{x}') \rangle &= \mathcal{K}_{GP_0}^L(\mathbf{x}, \mathbf{x}') - k_{GP_0}^L(\mathbf{x}) (K_{GP_0}^L)^{-1} k_{GP_0}^L(\mathbf{x}') \\ &+ \left[ (K_{NTK}^L)^{-1} k_{NTK}^L(\mathbf{x}) - (K_{GP_0}^L)^{-1} k_{GP_0}^L(\mathbf{x}) \right]^\top K_{GP_0}^L \left[ (K_{NTK}^L)^{-1} k_{NTK}^L(\mathbf{x}') - (K_{GP_0}^L)^{-1} k_{GP_0}^L(\mathbf{x}') \right] \end{aligned} \quad (27)$$

Finally, the correlation between the predictor at time  $t$  and  $t' = 0$  converges to the non-zero values.

$$\lim_{t \rightarrow \infty} \lim_{T \rightarrow 0} \sigma_0^{-2} \langle \delta f(t, \mathbf{x}) \delta f(0, \mathbf{x}') \rangle = \mathcal{K}_{GP_0}^L(\mathbf{x}, \mathbf{x}') - k_{NTK}^L(\mathbf{x})^\top (K_{NTK}^L)^{-1} k_{GP_0}^L(\mathbf{x}') \quad (28)$$

The fact that the correlation does not vanish signifies the strong dependence between the generalization and the random initial condition in deterministic gradient descent.

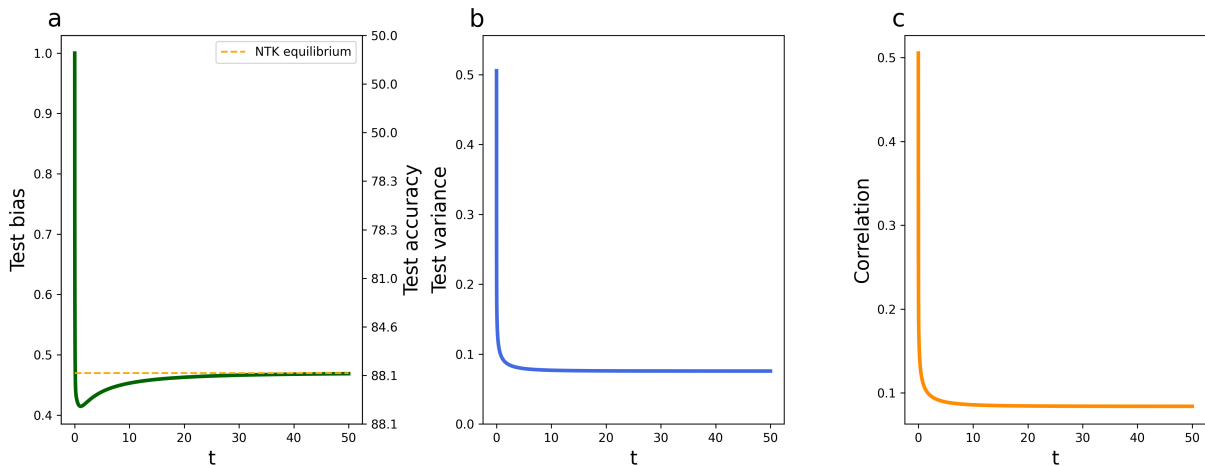


FIG. 3. Gradient Driven Phase: NTK theory for a ReLU deep network with one hidden layer. The network is trained on binary classification in CIFAR-10. (a) The dynamics of the test bias, defined as  $(\langle f(\mathbf{x}, t) \rangle - Y)^2$ , averaged over the test dataset, show convergence to the NTK equilibrium. (b) The variance of the predictor,  $\langle \delta f(t, \mathbf{x}) \delta f(t, \mathbf{x}) \rangle$ , averaged over the test dataset, decreases with learning to an equilibrium value (Eq.27). (c) The correlation with the initial condition,  $\langle \delta f(t, \mathbf{x}) \delta f(\mathbf{x}, 0) \rangle$ , do not vanish in the NTK equilibrium at long times but rather go to an equilibrium value (Eq.28). This implies that long-term generalization depends on the random initialization of weights in deterministic gradient descent process.

## B. Diffusive Dynamics

The diffusive regime is characterized by  $t \sim \mathcal{O}(1/T)$ . The SE loss at this stage is  $\mathcal{O}(T)$  as the network explores the solution subspace. The mean field equations (Eq.20-21) in this regime do not admit an analytical solution and have been solved numerically, with an exception of linear networks, where they are tractable. The numerical solutions are presented in Sec.VI. In linear networks, the NTK and the NNGP kernels are the same up to a constant, causing the mean predictor to remain fixed at the

NTK equilibrium value (to leading order in  $T$ ). The predictor covariance for linear networks takes the following simple form, at low temperatures and times of  $\mathcal{O}(1/T)$ :

$$\begin{aligned} \langle \delta f(t, \mathbf{x}) \delta f(t', \mathbf{x}') \rangle &= \\ m^{L+1}(t, t') \left[ \mathcal{K}_{in}(\mathbf{x}, \mathbf{x}') - k_{in}(\mathbf{x})^\top (K_{in})^{-1} k_{in}(\mathbf{x}') \right] \end{aligned} \quad (29)$$

Where  $\mathcal{K}_{in}(\mathbf{x}, \mathbf{x}') = \frac{1}{N_0} \mathbf{x} \cdot \mathbf{x}'$  is the input's covariance matrix. Similar to Sec.IV we define the  $P \times P$  matrix  $(K_{in})_{\mu\nu} = \mathcal{K}_{in}(\mathbf{x}_\mu, \mathbf{x}_\nu)$ , and the input  $P$  dimensional test vector as  $(k_{in}(\mathbf{x}))_\mu = \mathcal{K}_{in}(\mathbf{x}, \mathbf{x}_\mu)$ . During the

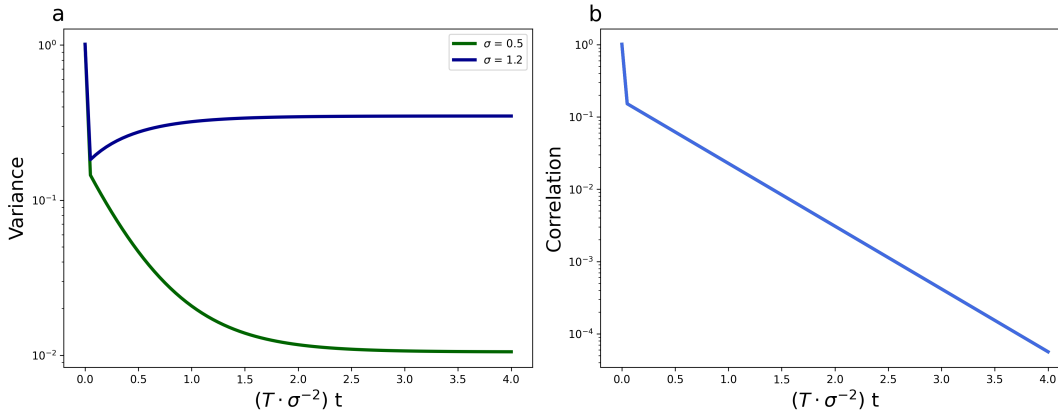


FIG. 4. Predictor Covariance in Linear Network: The theory of the predictor’s covariance in linear network during the diffusive phase (a) The variance of the predictor,  $\langle \delta f(t, \mathbf{x}) \delta f(t, \mathbf{x}) \rangle$ , averaged on the test dataset, is shown for two values of  $\sigma$  with  $\sigma_0 = 1$ . For  $\sigma < \sigma_0$ , the variance decreases during the diffusive learning phase due to the additional constraints imposed by  $L_2$  regularization. For  $\sigma > \sigma_0$ , the variance increases as the network explores the solution subspace. (b) The correlation with the initial condition,  $\langle \delta f(t, \mathbf{x}) \delta f(\mathbf{x}, 0) \rangle$ . A rapid decrease during the gradient-driven phase followed by an exponential decay in the diffusive learning phase, reflecting the decorrelation caused by random changes in the weights.

gradient-driven phase, the variance decreases as learning progresses, projecting the initial condition onto the subspace of zero training error. In the diffusive learning phase, the behavior of the variance depends on the ratio between  $\sigma$  and  $\sigma_0$ . When  $\sigma < \sigma_0$ , the variance is further reduced by the constraints of the  $L_2$  regularizer. When  $\sigma > \sigma_0$ , the variance increases as the weights explore the solution subspace with weaker constraints (see Fig. 4 (a)).

The correlation with the random initialization,  $\langle \delta f(t, \mathbf{x}) \delta f(\mathbf{x}, 0) \rangle$ , is shown in Fig.4 (b). In the NTK regime, this correlation remains  $\mathcal{O}(1)$  even at long times (see Eq.28), due to the strong dependence on the initial condition in the linearized dynamics. However, in the diffusive regime, the temporal correlation decays exponentially with a time scale of  $\sigma^2/T$  due to the stochastic nature of Langevin dynamics.

Another important limit is the equilibrium limit  $t \gg 1/T$ . In particular, the mean predictor reaches a constant value, given by looking for a constant solution to Eq.20 at  $t \rightarrow \infty$ , which together with Eq.16 yields

$$\lim_{t \rightarrow \infty} \langle f_{\text{train}}(t) \rangle = K_{GP}^L (IT\sigma^{-2} + K_{GP}^L)^{-1} Y \quad (30)$$

Similarly, for the test mean predictor,

$$\lim_{t \rightarrow \infty} \langle f(t, \mathbf{x}) \rangle = k_{GP}^L(\mathbf{x})^\top (IT\sigma^{-2} + K_{GP}^L)^{-1} Y \quad (31)$$

which agrees with the well-known equilibrium NNGP result [3]. We emphasize that Eqs.30-31 hold for any temperature.

## VI. NUMERICAL EVALUATIONS OF THE DYNAMIC MEAN FIELD EQUATIONS

In this section, we present the numerical solutions of the mean field Eqs.20-21, focusing on the mean-predictor in the diffusive phase, where  $t \sim \mathcal{O}(1/T)$ .

To analyze the dynamics’ dependence on the hyperparameters, we formally take the limit  $T \rightarrow 0$  of Eqs.20-21. We present the theoretical predictions for the test bias, defined as  $(\langle f(\mathbf{x}, t) \rangle - y(\mathbf{x}))^2$  and the resultant test accuracy on binary classification task in CIFAR-10 dataset (Fig.5). This accuracy can be thought of as taking the majority vote in an ensemble of neural networks trained on the same data. The methodology for solving the equations for low  $T$  is detailed in SI Sec.B5. As shown in Fig.5, the type of nonlinearity plays a significant role in shaping the learning process.

In ReLU kernels, varying  $\sigma$  and  $\sigma_0$  serves as a scaling factor without changing their structure. Notably, this indicates that both NTK and NNGP equilibria remain unchanged in ReLU networks regardless of  $\sigma$  and  $\sigma_0$ . Consequently, the start and end points of the diffusive learning phase are fixed and affected only by changing the data or the depth of the NN. However, altering the ratio between  $\sigma$  and  $\sigma_0$  can lead to qualitatively different dynamics and non-monotonous behavior, as demonstrated by the comparison of Fig.5 (c) and (d).

For error functions and other sigmoidal activation functions, the values of  $\sigma$  and  $\sigma_0$  induce a qualitative change in the dynamics, regardless of their ratio. With small  $\sigma$  and  $\sigma_0$ , the preactivations are small in magnitude, causing the sigmoidal function to behave almost linearly, which typically results in poor performance. In contrast, larger values of  $\sigma$  and  $\sigma_0$  increase the nonlin-

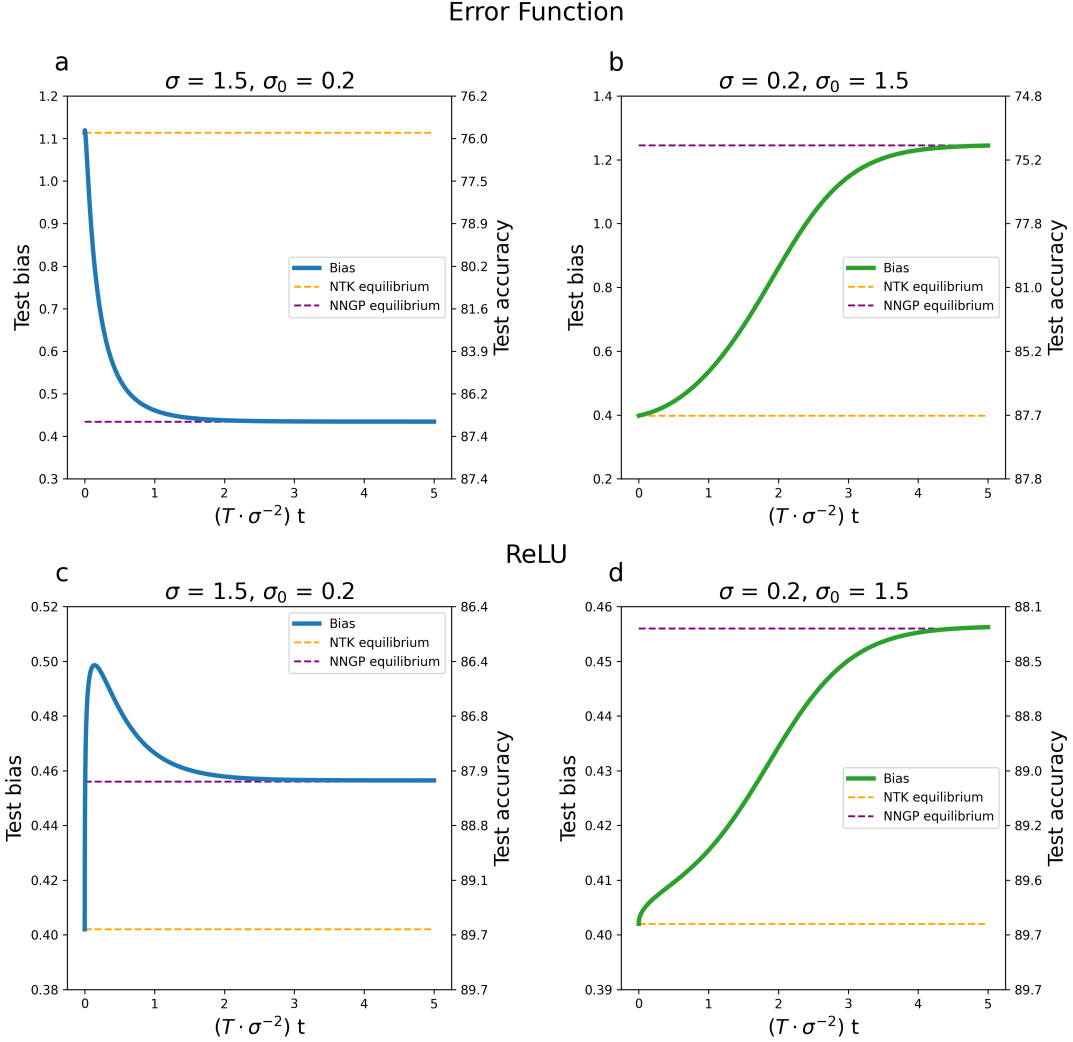


FIG. 5. Diffusive Dynamics: Numerical solutions of the mean field equations (Eqs.20- 21) in the diffusive phase, starting from the NTK equilibrium, which marks the end of the gradient-driven phase. We evaluated the test bias,  $\langle (f(\mathbf{x}, t) - y(\mathbf{x}))^2 \rangle$ , averaged over the test dataset for various nonlinear functions and parameters in a binary classification task in CIFAR-10. (a-b) Performance comparison with error function activation for different  $\sigma, \sigma_0$ . Small values cause the sigmoidal function to behave like a linear function, hindering the generalization. Large values lead to strong nonlinearity and improved performance. (a) Small  $\sigma_0$  and large  $\sigma$ . The accuracy after the exploratory diffusive phase is better by 10% compared to the gradient-driven phase. (b) Large  $\sigma_0$  and small  $\sigma$ . The accuracy after the gradient-driven phase is better by 12% compared to the equilibrium accuracy (c-d) Comparison of the performance with ReLU activation for different  $\sigma, \sigma_0$ . The values of the NTK and NNGP equilibria do not depend on the values of  $\sigma, \sigma_0$  (d) For  $\sigma_0$  and small  $\sigma$ , the accuracy converges monotonously to the NNGP equilibrium, while in (c) for large  $\sigma$  and small  $\sigma_0$  the learning is non-monotonic.

erity, often resulting in improved performance. In the binary classification task presented in Fig. 5(a-b), the test accuracy has improved by up to 12% by transitioning from small  $\sigma_0$  to large  $\sigma$  and vice versa.

## VII. NEURAL REPRESENTATIONS AND REPRESENTATIONAL DRIFT

We now explore the implications of diffusive learning dynamics on the phenomenon of representational drift.

Representational drift refers to the observations that neuronal activity patterns accumulate random changes over time without noticeable consequences for the relevant animal behavior [21, 34, 35]. These observations raise fundamental questions about the causal relation between neuronal representations and the underlying computation. Here we build on our analysis of the learning dynamics to study the nature of the representations in wide networks and the implications of their drift.

## A. Neuronal Representations

**Random weights:** Representation in our model refers to the patterns of activity of the neurons at the top hidden layer. In the wide networks studied here (with  $N^{-1/2}$  normalization), the hidden layer weights are only slightly modified by learning, resulting in weak feature learning. However, this does not mean that the representation itself is random. As is clear from the non-random structure of the kernels (Fig.2 above), the statistical structure of the inputs is reflected in the properties of the hidden neurons even after filtering by largely random weights. The kernel sums over the properties of all neurons in the layer; hence, even small statistical stimulus selectivity of individual neurons may result in a distinct structure of the kernel. It is, thus, important to examine the tuning properties of individual neurons. In fact, as shown in Fig.6, in high-dimensional inputs such as MNIST, the selectivity of individual representation neurons to class identity varies across input digits. For instance, it is pronounced for digits 0 and 1 but less so for digits 4 and 9. It is determined by the differences in amplitude for the classes, as will be discussed below (Sec. VIID). In contrast, when inputs are governed by low-dimensional statistical structure (Fig.7 (c)), the feature layer exhibits significant single neuron tuning curves similar to those observed in the cortex or hippocampus, even though hidden weights are completely random.

**Effect of learning:** Even in wide networks, hidden weights are not completely random and are affected by learning. This is clear from the derivation of the NDK where both changes in readout weights and hidden layer weights contribute to the kernel structure. Although these changes are small (of order  $N^{-1/2}$ ), they have a task-dependent low-rank structure, and hence they have  $\mathcal{O}(1)$  contribution to the predictor. Although the exact form of the learned-induced changes in the representation is complicated, elsewhere [30, 36, 37] we found that, at equilibrium, the changes in the representations  $\phi(\mathbf{z}^l(\mathbf{x}))$  can be approximated by  $\phi(\mathbf{z}^l(\mathbf{x})) \approx \phi_0(\mathbf{x}) + \frac{1}{\sqrt{N}}\mathbf{v}Y^\top$  where  $\phi_0(\mathbf{x})$  are the activations drawn from the prior distribution,  $\mathbf{v}$  is a Gaussian  $N_l$  dimensional vector with zero mean and variance  $\mathcal{O}(\sigma^{2L})$  and  $Y$  is the labels vector, as defined in Sec. II A.

## B. Representational Drift

Consider again the snapshot representation map shown in Fig.6 above. In Langevin dynamics, these tuning functions will gradually change over time due to the additive noise in the dynamics. Tracking a tuning curve during this process ultimately results in a random pattern (Fig.7 (a-d)). However, in any snapshot in time, the population statistics remain the same. Thus, by reordering the neurons, essentially the same tuning map reemerges (Fig.7

(e-h)), resembling observations in experimental data. It is interesting to note that the complete reordering of the representation also applies to the diffusion dynamics of the learned component of the representation. Specifically, the representational dynamics has approximately the form of

$$\phi(\mathbf{z}_t^l) \approx \phi(\mathbf{W}_0(t), \mathbf{x}) + N^{-1/2}\mathbf{v}(t)Y^\top \quad (32)$$

where  $\mathbf{W}_0(t)$  represents the time-dependent hidden layer weights, and the second term represents the low-rank 'feature learning' component. Both  $\mathbf{W}_0(t)$  and  $\mathbf{v}(t) \in \mathbb{R}^N$  obey the prior time-dependent statistics (Eq.6) and thus possess temporal correlations that decay exponentially to zero with a time scale of  $\sigma^2/T$ . Accordingly, even the dynamics of the learned features do not break the permutation symmetry and completely reorder the representation over time.

We have tested the reordering hypothesis by simulating a ReLU network with a single hidden layer and a single output, trained on CIFAR-10 binary classification with Langevin dynamics (Eq.5). We track the hidden layer representations on the training data  $\phi(\mathbf{z}_t(\mathbf{x}^\mu))$  during training. In order to characterize the drift phenomenon and reveal the low-rank structure, we compute the top right and left singular vectors of  $\phi(\mathbf{z}_t(\mathbf{x}^\mu))$ , denoted by  $h(t) \in \mathbb{R}^P$  and  $\mathbf{g}(t) \in \mathbb{R}^N$ , respectively, and track their cosine similarity after the dynamics reaches equilibrium in the diffusive learning stage. This time-dependent cosine similarity is defined as  $\rho_h(\tau) \equiv \lim_{t \rightarrow \infty} h(t+\tau)^\top h(t)$ , and  $\rho_g(\tau) \equiv \lim_{t \rightarrow \infty} \mathbf{g}(t+\tau)^\top \mathbf{g}(t)$ . As shown in Fig.8, we find that  $\rho_h(\tau)$  is stable during drift, while  $\mathbf{g}(t)$  gradually decorrelates over time, representing the drift in the  $N$ -dimensional feature space. This pattern is consistent with the low-rank learned-induced correction predicted by Eq.32.

## C. Stability of Computation

How does the system retain its functionality in the presence of constant reordering of the tuning of individual neurons? In our model, the stability of the input-output function of the network during the equilibrium diffusion phase is due to the continuous realignment of the readout weights  $\mathbf{a}(t)$  and the hidden layers weights  $\mathbf{W}(t)$  as they drift simultaneously, staying within the space of solutions as was suggested previously [23, 34, 35]. The above alignment scenario requires an ongoing learning signal acting on the weights, in the form of a weak ( $\mathcal{O}(T)$ ) gradient. In the absence of such a signal, the changes in the predictor due to the drift relative to an initial time  $t_0$  (in which the system has already achieved small error) is given by

$$\langle f(\mathbf{x}, t, t_0) \rangle = e^{-T\sigma^{-2}(t-t_0)} k^L(t, t_0, \mathbf{x})^\top (IT\sigma^{-2} + K_{GP}^L)^{-1} Y \quad (33)$$

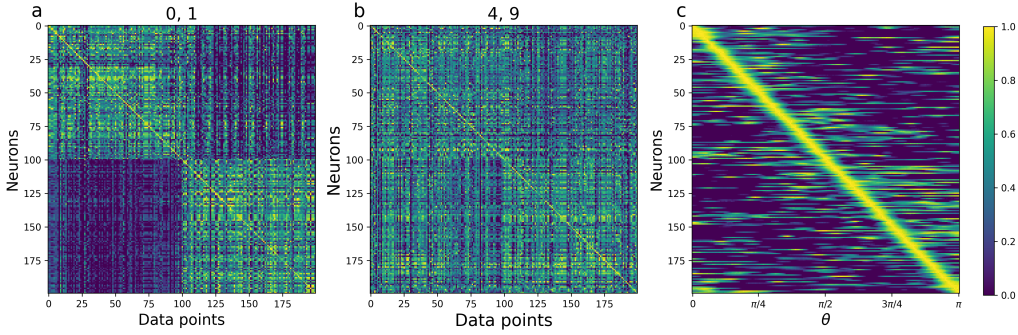


FIG. 6. Random Representations: The representations of a network with random Gaussian weights are presented for three cases: MNIST binary classification with the digits 0,1 (a), the digits 4,9 (b), and (c) for a data governed by a single scalar  $\theta$ , consists of a sum of harmonics with decaying amplitude (see SI Sec.H for details). For each data point the neuron with maximum activation was chosen, and the activations presented are normalized by their maximum value. (a) There is no selectivity of a single example, but rather a selectivity for class due to differences in class amplitude (see Sec.VII A). (b) No clear pattern emerges, and the two categories are indistinguishable. (c) A clear tuning curve pattern emerges because the data is governed by low-dimensional structure.

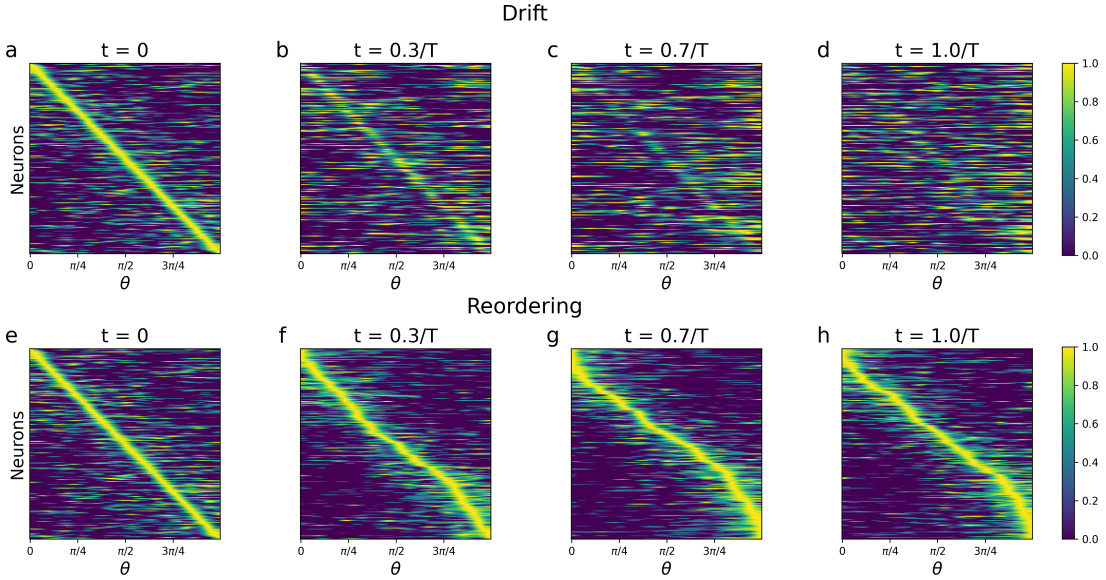


FIG. 7. Tuning Curves and Drift in Random Neural Networks: A deep ReLU network with one hidden layer and a Gaussian initial conditions, with weights drifting according to the prior dynamics (Eq.6), without learning constraints. The input data consists of a sum of harmonics with decaying amplitude (see Sec.H for details). (a,e) The tuning curve was constructed by selecting the neuron with maximum activation for each angle  $\theta$ , and normalized its activation. (a-d) The evolution of neuronal activations as they drift over time. The initial tuning curve gradually fades to a random pattern. (e-h) By reordering the same neurons during drift, a new tuning function emerges, due to the low dimensional structure of the data. This result resembles findings from experimental neuroscience [21].

where the exponential prefactor is due to decorrelation of the readout weights from their learned values at time  $t_0$ , resulting in an overall decay of the predictor to zero and chance level performance. The effect of decorrelation in the hidden layer weights is represented in the time-dependence of the kernel (see below).

We next consider an alternative scenario where the readout weights are frozen at their learned values at  $t_0$  while the weights of the hidden layers  $\mathbf{W}(t)$  continue to

drift without an external learning signal. We denote the output of the network in this scenario as  $f_{\text{drift}}(t, t_0, \mathbf{x})$ . Our theory predicts that the mean of  $f_{\text{drift}}(\mathbf{x}, t, t_0)$  (see SI Sec.F for details) is given by

$$\langle f_{\text{drift}}(t, t_0, \mathbf{x}) \rangle = k^L(t, t_0, \mathbf{x})^\top (IT\sigma^{-2} + K_{GP}^L)^{-1} Y \quad (34)$$

The kernel  $k^L(\mathbf{x}, t, t_0)$  represents the overlap between the

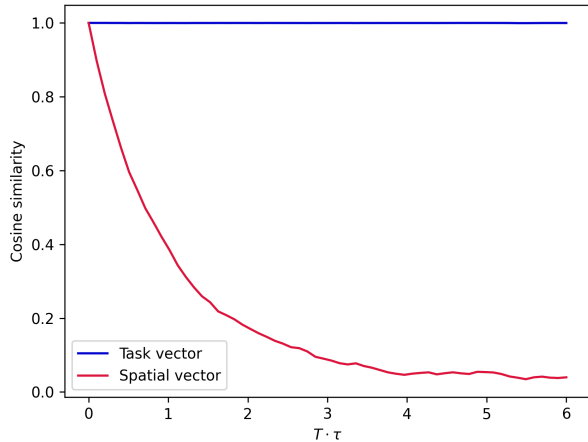


FIG. 8. Low Rank Structure and Drift: A ReLU network with a single hidden layer and a single output, trained on CIFAR-10 binary classification with Langevin dynamics (Eq.5). We analyze the SVD of the representation  $\phi(\mathbf{z}_t^L(\mathbf{x}))$ . We track the cosine similarity of the top right and left singular unit vectors, the  $P$ -dimensional task vector  $h(t)$  and the  $N$ -dimensional spatial vector  $\mathbf{g}(t)$ , respectively. The similarity of the  $P$ -dimensional vector remains stable during the drift process, while the similarity of the  $N$ -dimensional vector decay exponentially over time with a timescale of  $1/T$ , which is consistent with the low rank term in Eq.32.

top layer activations at time  $t_0$ , induced by the training inputs and that of a test point at time  $t$ . When  $t - t_0$  is large, the two representations completely decorrelate and the predictor is determined by the 'mean' kernel function

$$\mathcal{K}_{mean}^L(\mathbf{x}, \mathbf{x}') = \frac{1}{N_L} \langle \phi(\mathbf{z}^L(\mathbf{x})) \rangle_0 \cdot \langle \phi(\mathbf{z}^L(\mathbf{x}')) \rangle_0 \quad (35)$$

which is a modified version of the NNGP kernel where the Gaussian averages are performed separately for each data point. Thus, the long time limit of the mean predictor in this scenario is

$$\lim_{t-t_0 \rightarrow \infty} \langle f_{\text{drift}}(t, t_0, \mathbf{x}) \rangle = k_{mean}^L(\mathbf{x})^\top (IT\sigma^{-2} + K_{GP}^L)^{-1} Y \quad (36)$$

where  $k_{mean}^L(\mathbf{x})$  is defined as applying the mean kernel function to the test data. In this scenario, the predictor does not necessarily decay to chance level, as discussed in the next section.

#### D. Invariant Code

It has been hypothesized that the observed stability of the network function against the drift process is due to the fact that the readout utilizes a representational feature which is invariant to permutation of the neurons

[17, 18, 21, 38–40]. A simple example would be the case where the statistics of the population firing rates (e.g., mean firing rate) is modulated by the stimulus. Does our network exhibit a representational code which is invariant to the random sampling of the hidden weights over long times? The answer depends on both the type of non-linearity of the hidden layer neurons and the nature of the task. Above, we have shown that any information about the input which is invariant to the weight sampling should be contained in the mean-kernel, see Eq.35. For odd nonlinearities (e.g., linear and error function activations),  $\mathcal{K}_{mean}^L(\mathbf{x}, \mathbf{x}')$  is identically zero. However, this is not true for other nonlinearities (e.g., ReLU) where the mean activity remains non-zero. Since the distribution of the preactivations is symmetric around zero, it is invariant to the sign of the input activations, hence it cannot encode any task information embedded in the first moment of the inputs. However, the mean post activation does depend on the norm of the input vectors,  $\|\mathbf{x}\|$  and  $\|\mathbf{x}'\|$ , as mentioned in Sec.IV and can be seen in Fig.2 (f) above. As a result, if the distribution of the norms carries information relevant to the given task, the predictor can retain significant information despite the drift. On the other hand, if the norms of the inputs are not modulated in a task-dependent manner, the decorrelated representations yield chance-level performance.

We present examples illustrating both scenarios in Fig.9. Specifically, we consider two MNIST binary classification tasks after reaching the long-time equilibrium. For each task, we show the evolution of the histograms of the predictor on the training examples at time  $t$ , after freezing the readout weights at an earlier time  $t_0$ . To evaluate the amount of discriminability retained in the predictor histograms, we evaluated the classification accuracy given by the optimal separating threshold (see SI Sec.H for details). In the case of digits 4 and 9, the two histograms eventually overlap, resulting in long-time chance-level accuracy and a complete loss of the learned information. In contrast, for the digits 0 and 1 (Fig. 9(f-j)), the histograms of the two classes remain partially separated, leading to a long-time accuracy of 90%, which reflects the residual information contained in the input norms. Interestingly, during the transition from the initial state to the long-time state, the distributions temporarily cross, causing a brief period of chance performance.

Additional architectural biases can be leveraged to enhance the stability of function. As an example, we consider feedforward networks with local receptive fields (as in convolutional networks). With such constraints, even if the overall amplitude of an example is not informative of the class, the local amplitude, i.e., the  $L_2$  norm of the inputs within a receptive field of each representation neuron, may carry information about the task, which will be preserved in the 'mean-kernel'. In Fig. 10, we demonstrate that reducing the receptive field allows the overlapping distributions of digits 4 and 9 to become separable. The highest accuracy is achieved with a re-

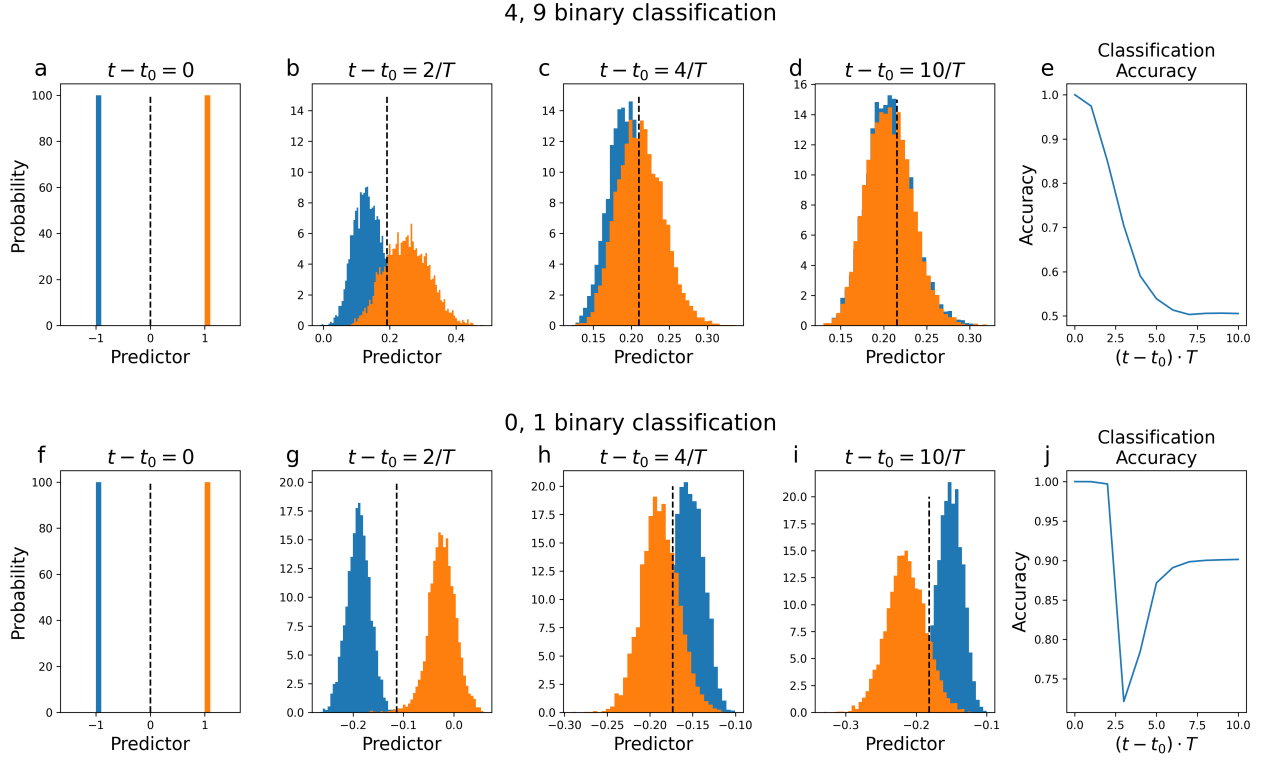


FIG. 9. Representational Drift with Fixed Readout Weights After Learning: (a-d, f-i) The histogram of the predictor during drift,  $f_{\text{drift}}(\mathbf{x}, t, t_0)$ , on the training data. (a,f) Initially, there is perfect class separation at  $\pm 1$ . Performance gradually deteriorates as the readout weights  $\mathbf{a}(t_0)$  and the hidden layer weights  $\mathbf{W}(t)$  lose alignment due to drift. In the classification task involving digits 0 and 1, the histogram is still separable after complete decorrelation, due to differences in the class norms (see Sec.VIID). In the classification task of the digits 4 and 9, performance declines to chance level. (e, j) The classification accuracy using an optimal threshold is plotted as a function of the time difference from the freezing time  $t_0$ .

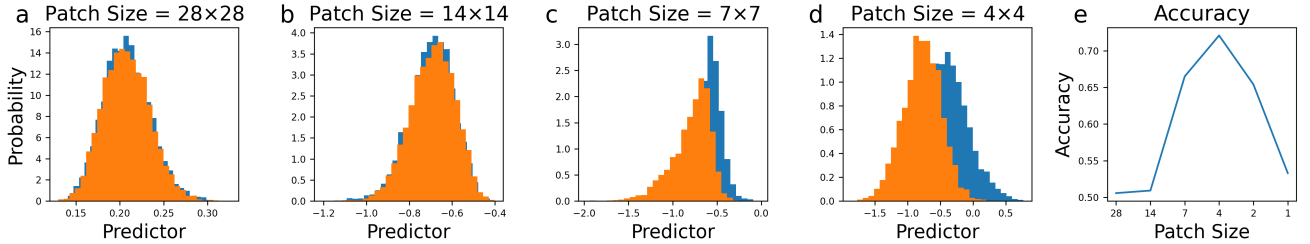


FIG. 10. Architectural Bias: We demonstrate how limiting the receptive field (via convolution) can enhance performance after drift. Each neuron in the network receives input from a fixed patch from the total image, and we vary patch size (the total image is  $28 \times 28$ ). (a-d) The histograms are more separable when the receptive field is limited, with an optimal patch size of  $4 \times 4$ . (e) The accuracy measured by an optimal threshold reaches 72% compared to chance-level with an unlimited receptive field. The limited receptive field emphasizes class differences, as the norms of small patches exhibit greater variability between classes than the norms of the entire image. Importantly, if the patch size is too small, structural information about the image is lost, leading to poor performance.

ceptive field of  $4 \times 4$  pixels, increasing performance from chance level to 72%. When the receptive field becomes too small, the spatial structure of the digits is lost, and the performance is poor again. We stress that the limited receptive field breaks the permutation symmetry between neurons, and thus the drift process does not act as

a complete reordering like was observed with unlimited receptive field in Fig.7. In biological circuits with limited receptive fields, this symmetry breaking may play a role in retaining computation in the presence of drift.

### VIII. DISCUSSION

Our work provides a theoretical framework for the complete trajectory of gradient descent learning dynamics in wide deep neural networks in the presence of small noise, unifying the NTK theory and the NNGP theory as two limits of the same underlying process. The dynamics is captured by the time-dependent Neural Dynamical Kernel (NDK), a dynamical generalization of the NTK. Although noise is externally introduced in our setup, stochasticity in practical machine learning often arises from the random sampling of examples in mini-batches (such as in SGD). We speculate that the insights from current theory may be relevant to this types of noise as well [41–44].

The theory provides new insights into the learning dynamics during the diffusive learning phase, where the learning process explores the solution space. We focus on characterizing commonly used activation functions and elucidating their interactions with other hyperparameters. In particular, we highlight the impact of  $\sigma_0^2$  and  $\sigma^2$ , which correspond to the variance of the weights at initialization and that of the Bayesian prior regularization, respectively. These parameters play a pivotal role in shaping the trajectories of the predictor and the time scales of the different stages of the learning dynamics. We demonstrate that for sigmoidal activation functions, the values of these variances may substantially affect the learning trajectory and performance. Small weight variance leads to linear-like behavior and poor generalization, whereas large values induce strong nonlinearity and typically result in improved performance. As a result, large differences in the two variances may cause drastic changes in behavior across time as the system moves from being dominated by the initial weights to the diffusive stage dominated by the prior regularization. These insights can be utilized in practical machine-learning applications.

Our Bayesian framework provides a model of representational drift where the weights undergo random drifts which are compensated by continuous realignment of the hidden and readout weights, keeping the system in the solution space, as was previously suggested [34, 35]. In our Langevin learning dynamics, this realignment is due to the presence of an ongoing learning signal, which is nonzero even at the equilibrium stage. The source of the putative realignment signals in brain circuits is unclear. An alternative hypothesis is that the computation in neuronal circuits is based on representational features that are invariant to the drift process [17, 18, 21, 38–40]. We show that in our framework, this scenario requires (1) that the readout weights are frozen after learning and (2) that task-relevant information impacts the structure of the representation kernel even after its decorrelation (the ‘mean-kernel’, Eq. 35). We provide examples of such features and illustrate how invariant codes can be enhanced by appropriate architectural biases that further constrain the drift.

So far, we have focused on learning in infinitely wide networks in the lazy regime, where the time dependence of the NDK arises from random drift in the solution space. Learning dynamics in finite width networks or in infinite width networks with non-lazy architecture are likely more complex [45–49]. Previous works have also extended the equilibrium theory of Bayesian learning to lazy and non-lazy networks in which data size is proportional to the network width [30, 36, 50–52]. It will be important to generalize the current dynamical theory to capture these architectures and regimes.

**Acknowledgments:** We thank the anonymous reviewers for their helpful comments. This research is supported by the Gatsby Charitable Foundation, the Swartz Foundation, ONR grant No.N0014-23-1-2051, and the Kempner Institute for the Study of Natural and Artificial Intelligence.

- 
- [1] T. Hazan and T. Jaakkola, Steps toward deep kernel methods from infinite neural networks, arXiv preprint arXiv:1508.05133 (2015).
- [2] A. Jacot, F. Gabriel, and C. Hongler, Neural tangent kernel: Convergence and generalization in neural networks, *Advances in neural information processing systems* **31** (2018).
- [3] J. Lee, J. Sohl-dickstein, J. Pennington, R. Novak, S. Schoenholz, and Y. Bahri, Deep neural networks as gaussian processes, in *International Conference on Learning Representations* (2018).
- [4] J. Lee, L. Xiao, S. Schoenholz, Y. Bahri, R. Novak, J. Sohl-Dickstein, and J. Pennington, Wide neural networks of any depth evolve as linear models under gradient descent, *Advances in neural information processing systems* **32** (2019).
- [5] A. G. d. G. Matthews, M. Rowland, J. Hron, R. E. Turner, and Z. Ghahramani, Gaussian process behaviour in wide deep neural networks, arXiv preprint arXiv:1804.11271 (2018).
- [6] R. M. Neal, Priors for infinite networks (tech. rep. no. crg-tr-94-1), University of Toronto **415** (1994).
- [7] R. Novak, L. Xiao, J. Lee, Y. Bahri, G. Yang, J. Hron, D. A. Abolafia, J. Pennington, and J. Sohl-Dickstein, Bayesian deep convolutional networks with many channels are gaussian processes, arXiv preprint arXiv:1810.05148 (2018).
- [8] R. Novak, L. Xiao, J. Hron, J. Lee, A. A. Alemi, J. Sohl-Dickstein, and S. S. Schoenholz, Neural tangents: Fast and easy infinite neural networks in python, arXiv preprint arXiv:1912.02803 (2019).
- [9] J. Sohl-Dickstein, R. Novak, S. S. Schoenholz, and J. Lee, On the infinite width limit of neural networks with a standard parameterization, arXiv preprint arXiv:2001.07301 (2020).
- [10] C. Williams, Computing with infinite networks, *Advances in neural information processing systems* **9** (1996).
- [11] G. Yang, Wide feedforward or recurrent neural networks of any architecture are gaussian processes, *Advances in Neural Information Processing Systems* **32** (2019).
- [12] L. Chizat and F. Bach, Implicit bias of gradient descent for wide two-layer neural networks trained with the logistic loss, in *Conference on Learning Theory* (PMLR, 2020) pp. 1305–1338.
- [13] H. Jin and G. Montúfar, Implicit bias of gradient descent for mean squared error regression with wide neural networks, arXiv preprint arXiv:2006.07356 (2020).
- [14] H. Min, S. Tarmoun, R. Vidal, and E. Mallada, On the explicit role of initialization on the convergence and implicit bias of overparametrized linear networks, in *International Conference on Machine Learning* (PMLR, 2021) pp. 7760–7768.
- [15] Y. Cho and L. Saul, Kernel methods for deep learning, *Advances in neural information processing systems* **22** (2009).
- [16] J. Lee, S. Schoenholz, J. Pennington, B. Adlam, L. Xiao, R. Novak, and J. Sohl-Dickstein, Finite versus infinite neural networks: an empirical study, *Advances in Neural Information Processing Systems* **33**, 15156 (2020).
- [17] D. Deitch, A. Rubin, and Y. Ziv, Representational drift in the mouse visual cortex, *Current biology* **31**, 4327 (2021).
- [18] T. D. Marks and M. J. Goard, Stimulus-dependent representational drift in primary visual cortex, *Nature communications* **12**, 5169 (2021).
- [19] U. Rokni, A. G. Richardson, E. Bizzi, and H. S. Seung, Motor learning with unstable neural representations, *Neuron* **54**, 653 (2007).
- [20] C. E. Schoonover, S. N. Ohashi, R. Axel, and A. J. Fink, Representational drift in primary olfactory cortex, *Nature* **594**, 541 (2021).
- [21] M. E. Rule, T. O’Leary, and C. D. Harvey, Causes and consequences of representational drift, *Current opinion in neurobiology* **58**, 141 (2019).
- [22] S. Qin, S. Farashahi, D. Lipshutz, A. M. Sengupta, D. B. Chklovskii, and C. Pehlevan, Coordinated drift of receptive fields in hebbian/anti-hebbian network models during noisy representation learning, *Nature Neuroscience*, 1 (2023).
- [23] P. Masset, S. Qin, and J. A. Zavatone-Veth, Drifting neuronal representations: Bug or feature?, *Biological Cybernetics* **116**, 253 (2022).
- [24] W. Coffey and Y. P. Kalmykov, *The Langevin equation: with applications to stochastic problems in physics, chemistry and electrical engineering*, Vol. 27 (World Scientific, 2012).
- [25] M. Welling and Y. W. Teh, Bayesian learning via stochastic gradient langevin dynamics, in *Proceedings of the 28th international conference on machine learning (ICML-11)* (2011) pp. 681–688.
- [26] R. Shwartz-Ziv and N. Tishby, Opening the black box of deep neural networks via information, arXiv preprint arXiv:1703.00810 (2017).
- [27] A. Ratzon, D. Derdikman, and O. Barak, Representational drift as a result of implicit regularization, *Elife* **12**, RP90069 (2024).
- [28] A. Krogh and J. Hertz, A simple weight decay can improve generalization, *Advances in neural information processing systems* **4** (1991).
- [29] T. Galanti, Z. S. Siegel, A. Gupte, and T. Poggio, Characterizing the implicit bias of regularized sgd in rank minimization, *CoRR*, abs/2206.05794 v6 (2022).
- [30] Q. Li and H. Sompolinsky, Statistical mechanics of deep linear neural networks: The backpropagating kernel renormalization, *Physical Review X* **11**, 031059 (2021).
- [31] G. E. Uhlenbeck and L. S. Ornstein, On the theory of the brownian motion, *Physical review* **36**, 823 (1930).
- [32] A. Krizhevsky, V. Nair, and G. Hinton, The cifar-10 dataset, online: <http://www.cs.toronto.edu/kriz/cifar.html> **55** (2014).
- [33] R. Kubo, The fluctuation-dissipation theorem, *Reports on progress in physics* **29**, 255 (1966).
- [34] M. E. Rule, A. R. Loback, D. V. Raman, L. N. Driscoll, C. D. Harvey, and T. O’Leary, Stable task information from an unstable neural population, *Elife* **9**, e51121 (2020).
- [35] M. E. Rule and T. O’Leary, Self-healing codes: How stable neural populations can track continually reconfiguring neural representations, *Proceedings of the National Academy of Sciences* **119**, e2106692119 (2022).
- [36] Q. Li and H. Sompolinsky, Globally gated deep linear networks, arXiv preprint arXiv:2210.17449 (2022).
- [37] Q. Li, B. Sorscher, and H. Sompolinsky, Representations

- and generalization in artificial and brain neural networks, *Proceedings of the National Academy of Sciences* **121**, e2311805121 (2024).
- [38] A. Rubin, L. Sheintuch, N. Brande-Eilat, O. Pinchasof, Y. Rechavi, N. Geva, and Y. Ziv, Revealing neural correlates of behavior without behavioral measurements, *Nature communications* **10**, 4745 (2019).
- [39] S. Druckmann and D. B. Chklovskii, Neuronal circuits underlying persistent representations despite time varying activity, *Current Biology* **22**, 2095 (2012).
- [40] M. T. Kaufman, M. M. Churchland, S. I. Ryu, and K. V. Shenoy, Cortical activity in the null space: permitting preparation without movement, *Nature neuroscience* **17**, 440 (2014).
- [41] J. Wu, W. Hu, H. Xiong, J. Huan, V. Braverman, and Z. Zhu, On the noisy gradient descent that generalizes as sgd, in *International Conference on Machine Learning* (PMLR, 2020) pp. 10367–10376.
- [42] H. Noh, T. You, J. Mun, and B. Han, Regularizing deep neural networks by noise: Its interpretation and optimization, *Advances in Neural Information Processing Systems* **30** (2017).
- [43] F. Mignacco and P. Urbani, The effective noise of stochastic gradient descent, *Journal of Statistical Mechanics: Theory and Experiment* **2022**, 083405 (2022).
- [44] A. Dalalyan, Further and stronger analogy between sampling and optimization: Langevin monte carlo and gradient descent, in *Conference on Learning Theory* (PMLR, 2017) pp. 678–689.
- [45] H. Shan and B. Bordelon, A theory of neural tangent kernel alignment and its influence on training, arXiv preprint arXiv:2105.14301 (2021).
- [46] N. Vyas, Y. Bansal, and P. Nakkiran, Limitations of the ntk for understanding generalization in deep learning, arXiv preprint arXiv:2206.10012 (2022).
- [47] A. Canatar and C. Pehlevan, A kernel analysis of feature learning in deep neural networks, in *2022 58th Annual Allerton Conference on Communication, Control, and Computing (Allerton)* (IEEE, 2022) pp. 1–8.
- [48] B. Bordelon and C. Pehlevan, Self-consistent dynamical field theory of kernel evolution in wide neural networks, arXiv preprint arXiv:2205.09653 (2022).
- [49] T. Flesch, K. Juechems, T. Dumbalska, A. Saxe, and C. Summerfield, Orthogonal representations for robust context-dependent task performance in brains and neural networks, *Neuron* **110**, 1258 (2022).
- [50] A. van Meeegen and H. Sompolinsky, Coding schemes in neural networks learning classification tasks, arXiv preprint arXiv:2406.16689 (2024).
- [51] B. Woodworth, S. Gunasekar, J. D. Lee, E. Moroshko, P. Savarese, I. Golan, D. Soudry, and N. Srebro, Kernel and rich regimes in overparametrized models, in *Conference on Learning Theory* (PMLR, 2020) pp. 3635–3673.
- [52] S. Azulay, E. Moroshko, M. S. Nacson, B. E. Woodworth, N. Srebro, A. Globerson, and D. Soudry, On the implicit bias of initialization shape: Beyond infinitesimal mirror descent, in *International Conference on Machine Learning* (PMLR, 2021) pp. 468–477.
- [53] M. Mézard, G. Parisi, and M. A. Virasoro, *Spin glass theory and beyond: An Introduction to the Replica Method and Its Applications*, Vol. 9 (World Scientific Publishing Company, 1987).
- [54] S. Franz, G. Parisi, and M. A. Virasoro, The replica method on and off equilibrium, *Journal de Physique I* **2**, 1869 (1992).
- [55] E. Gardner, The space of interactions in neural network models, *Journal of physics A: Mathematical and general* **21**, 257 (1988).
- [56] M. Gabrié, A. Manoel, C. Luneau, N. Macris, F. Krzakala, L. Zdeborová, *et al.*, Entropy and mutual information in models of deep neural networks, *Advances in Neural Information Processing Systems* **31** (2018).
- [57] G. Carleo, I. Cirac, K. Cranmer, L. Daudet, M. Schuld, N. Tishby, L. Vogt-Maranto, and L. Zdeborová, Machine learning and the physical sciences, *Reviews of Modern Physics* **91**, 045002 (2019).
- [58] Y. Bahri, J. Kadmon, J. Pennington, S. S. Schoenholz, J. Sohl-Dickstein, and S. Ganguli, Statistical mechanics of deep learning, *Annual Review of Condensed Matter Physics* **11**, 501 (2020).
- [59] L. Saglietti and L. Zdeborová, Solvable model for inheriting the regularization through knowledge distillation, in *Mathematical and Scientific Machine Learning* (PMLR, 2022) pp. 809–846.
- [60] N. Parikh, S. Boyd, *et al.*, Proximal algorithms, *Foundations and trends® in Optimization* **1**, 127 (2014).
- [61] N. G. Polson, J. G. Scott, and B. T. Willard, Proximal algorithms in statistics and machine learning, arXiv preprint arXiv:1502.07944 (2015).
- [62] M. Teboulle, Convergence of proximal-like algorithms, *SIAM Journal on Optimization* **7**, 1069 (1997).
- [63] D. Drusvyatskiy and A. S. Lewis, Error bounds, quadratic growth, and linear convergence of proximal methods, *Mathematics of Operations Research* **43**, 919 (2018).
- [64] H. Robbins and S. Monro, A stochastic approximation method, *The annals of mathematical statistics* , 400 (1951).
- [65] S.-I. Amari, Natural gradient works efficiently in learning, *Neural computation* **10**, 251 (1998).
- [66] A. Beck and M. Teboulle, Mirror descent and nonlinear projected subgradient methods for convex optimization, *Operations Research Letters* **31**, 167 (2003).
- [67] J. Bae, P. Vicol, J. Z. HaoChen, and R. B. Grosse, Amortized proximal optimization, *Advances in Neural Information Processing Systems* **35**, 8982 (2022).
- [68] H. Shan, Q. Li, and H. Sompolinsky, Order parameters and phase transitions of continual learning in deep neural networks, arXiv preprint arXiv:2407.10315 (2024).
- [69] S. Franz and G. Parisi, Effective potential in glassy systems: theory and simulations, *Physica A: Statistical Mechanics and its Applications* **261**, 317 (1998).

# Supplemental Information

## Appendix A: Markov Proximal Learning

We introduce a Markov Proximal Learning (MPL) framework for learning dynamics in fully connected Deep Neural Networks (DNNs). This method allows us to construct a dynamical mean field theory for Langevin dynamics in the infinite width limit, and is a novel way to discretize Langevin dynamics and formulate out-of-equilibrium statistical mechanics. We formally write down the moment-generating function (MGF) of the predictor. We then use the well-known replica method in statistical physics [53, 54], which has also been shown to be a powerful tool for deriving analytical results for learning in NNs [55–59]. We analytically calculate the MGF after averaging over the posterior distribution of the network weights in the infinite width limit, which enables us to compute statistics of the predictor.

### 1. Definition of Markov Proximal Learning

We consider the network learning dynamics as a Markov proximal process, which is a generalized version of the *deterministic* proximal algorithm ([60, 61]). Deterministic proximal algorithm with  $L_2$  regularization is a sequential update rule defined as

$$\Theta_t(\Theta_{t-1}, \mathcal{D}) = \arg \min_{\Theta} \left( E(\Theta|\mathcal{D}) + \frac{\lambda}{2} |\Theta - \Theta_{t-1}|^2 \right) \quad (\text{A1})$$

where  $\lambda$  is a parameter determining the strength of the proximity constraint. This algorithm has been proven to converge to the global minimum for convex cost functions [62, 63], and many optimization algorithms widely used in machine learning can be seen as its approximations [64–67]. We define a stochastic extension of proximal learning, the Markov proximal learning. This method was also inspired by continual learning methods [68] and Franz-Parisi potential [69]. The process is characterized by the following transition matrix

$$\mathcal{T}(\Theta_t|\Theta_{t-1}) = \frac{1}{Z(\Theta_{t-1})} \exp \left( -\frac{1}{2} \beta \left( E(\Theta_t) + \frac{\lambda}{2} |\Theta_t - \Theta_{t-1}|^2 \right) \right) \quad (\text{A2})$$

where  $Z(\Theta_{t-1})$  is the single-time partition function, which imposes normalization throughout the Markov process,  $Z(\Theta_{t-1}) = \int d\Theta' \exp \left( -\frac{1}{2} \beta \left( E(\Theta') + \frac{\lambda}{2} |\Theta' - \Theta_{t-1}|^2 \right) \right)$ .  $\beta$  is an inverse temperature parameter characterizing the level of ‘uncertainty’ and  $\beta \rightarrow \infty$  limit recovers the deterministic proximal algorithm. We note that in the large  $\lambda$  limit, the difference between  $\Theta_t$  and  $\Theta_{t-1}$  is infinitesimal, and  $\Theta_t$  becomes a smooth function of continuous time, where the time variable is the discrete time divided by  $\lambda$ .

The joint probability of the parameters is given by  $(\Theta_0, \Theta_1, \dots, \Theta_t)$ .

$$P(\Theta_0, \Theta_1, \dots, \Theta_t) = \left[ \prod_{\tau=1}^t \mathcal{T}(\Theta_\tau|\Theta_{\tau-1}) \right] P(\Theta_0) \quad (\text{A3})$$

where  $P(\Theta_0)$  is the distribution of the initial condition of the parameters.

### 2. Large $\lambda$ Limit and Langevin dynamics:

We prove that in the limit of large  $\lambda$  and differentiable cost function this algorithm is equivalent to Langevin dynamics. We define  $\delta\Theta_t = \Theta_t - \Theta_{t-1}$ . In the limit of large  $\lambda$ , we can expand the transition matrix around  $\delta\Theta_t = 0$ :

$$\mathcal{T}(\delta\Theta_t|\Theta_{t-1}) \approx \left( \frac{\lambda\beta}{4\pi} \right)^{\frac{d}{2}} \exp \left[ -\frac{\lambda\beta}{4} \left| \delta\Theta_t + \frac{1}{\lambda} \nabla E(\Theta_{t-1}) \right|^2 \right] \quad (\text{A4})$$

$\delta\Theta_t|\Theta_{t-1}$  is a Gaussian random variable with the statistics:

$$\langle \delta\Theta_t|\Theta_{t-1} \rangle = -\frac{1}{\lambda} \nabla_{\Theta} E(\Theta_{t-1}) \quad (\text{A5})$$

$$\text{var}(\delta\Theta_t \delta\Theta_{t'}^\top | \Theta_{t-1}) = \frac{2}{\lambda\beta} \delta_{t,t'} I \quad (\text{A6})$$

which is equivalent to Langevin dynamics in Itô discretization:

$$\delta\Theta_t = (-\nabla_{\Theta} E(\Theta_{t-1}) + \eta_{t-1}) dt \quad (\text{A7})$$

with

$$\langle \eta_t \eta_{t'}^\top \rangle = \frac{2T}{dt} \delta_{t,t'} I, \langle \eta_t \rangle = 0 \quad (\text{A8})$$

where  $\frac{1}{\lambda} = dt, \beta = \frac{1}{T}$ .

## Appendix B: The Statistics of the Predictor

### 1. Replica Calculation of the Moment-Generating Function of the Predictor

The transition density can be written using the replica method, where  $Z^{-1}(\Theta_{t-1}) = \lim_{n \rightarrow 0} Z^{n-1}(\Theta_{t-1})$ :

$$\begin{aligned} \mathcal{T}(\Theta_t | \Theta_{t-1}) &= \lim_{n \rightarrow 0} Z^{n-1}(\Theta_{t-1}) \exp\left(-\frac{1}{2}\beta \left(E(\Theta_t) + \frac{\lambda}{2} |\Theta_t - \Theta_{t-1}|^2\right)\right) \\ &= \lim_{n \rightarrow 0} \prod_{\alpha=1}^{n-1} \int d\Theta_t^\alpha \exp\left(-\frac{\beta}{2} \left(\sum_{\alpha=1}^n E(\Theta_t^\alpha) + \frac{\lambda}{2} \sum_{\alpha=1}^n |\Theta_t^\alpha - \Theta_{t-1}^\alpha|^2\right)\right) \end{aligned} \quad (\text{B1})$$

Here  $\alpha = 1, \dots, n-1$  are the 'replicated copies' of the physical variable  $\{\Theta_\tau^n\}_{\tau=1, \dots, t}$ . To calculate the statistics of the dynamical process, we consider the MGF for arbitrary functions of the trajectory  $g(\{\Theta_\tau^n\}_{\tau=0, \dots, t})$

$$\begin{aligned} \mathcal{M}[\ell] &= \left\langle \exp\left(\sum_{t=1}^{\infty} \ell_t g(\{\Theta_\tau^n\}_{\tau=0, \dots, t})\right) \right\rangle_{\Theta} \\ &= \prod_{\tau=0}^{\infty} \int d\Theta_\tau \left[ \prod_{\tau=1}^{\infty} \mathcal{T}(\Theta_\tau | \Theta_{\tau-1}) \right] P(\Theta_0) \exp\left(\sum_{t=1}^{\infty} \ell_t g(\{\Theta_\tau^n\}_{\tau=0, \dots, t})\right) \\ &= \lim_{n \rightarrow 0} \prod_{\alpha=1}^n \prod_{\tau=1}^{\infty} \int d\Theta_t^\alpha \int d\Theta_0^n P(\Theta_0^n) \\ &\quad \exp\left(-\frac{\beta}{2} \sum_{\tau=1}^{\infty} \left(\sum_{\alpha=1}^n E(\Theta_\tau^\alpha) + \frac{\lambda}{2} \sum_{\alpha=1}^n |\Theta_\tau^\alpha - \Theta_{\tau-1}^\alpha|^2\right) + \sum_{t=1}^{\infty} \ell_t g(\{\Theta_\tau^n\}_{\tau=0, \dots, t})\right) \end{aligned} \quad (\text{B2})$$

We apply this formalism to the supervised learning cost function introduced in Sec.II A in the main text.

$$E(\Theta_t | \mathcal{D}) = \frac{1}{2} \sum_{\mu=1}^P (f(\mathbf{x}^\mu, \Theta_t) - y^\mu)^2 + \frac{T}{2\sigma^2} |\Theta_t|^2 \quad (\text{B3})$$

and the predictor statistics at time  $t$ ,  $g(\{\Theta_\tau^n\}_{\tau=0, \dots, t}) = f(\mathbf{x}, \Theta_t^n)$ , yielding

$$\mathcal{M}[\ell] = \lim_{n \rightarrow 0} \prod_{\alpha=1}^n \prod_{\tau=1}^{\infty} \int d\Theta_\tau^\alpha \int d\Theta_0 \exp\left(-\frac{\beta}{4} \sum_{\tau=1}^{\infty} \sum_{\alpha=1}^n (f_{\text{train}}(\Theta_\tau^\alpha) - Y)^2 + \sum_{t=1}^{\infty} \sum_{\mathbf{x}} \ell_{t,\mathbf{x}} f(\mathbf{x}, \Theta_t^n) - S_0[\Theta]\right) \quad (\text{B4})$$

$$S_0[\Theta] = \frac{1}{4} \sum_{\tau=1}^{\infty} \sum_{\alpha=1}^n \left(\sigma^{-2} |\Theta_\tau^\alpha|^2 + \lambda\beta |\Theta_\tau^\alpha - \Theta_{\tau-1}^\alpha|^2\right) + \frac{1}{2} \sigma_0^{-2} |\Theta_0^n|^2 \quad (\text{B5})$$

Where we define  $f_{\text{train}}(\Theta_\tau^\alpha) \equiv [f(\mathbf{x}^1, \Theta_\tau^\alpha), \dots, f(\mathbf{x}^P, \Theta_\tau^\alpha)]^T \in \mathbb{R}^P$  a vector contains the predictor on the training dataset, and  $Y \in \mathbb{R}^P$  such that  $Y^\mu = y^\mu$ , similar to Sec.II A.  $S_0[\Theta]$  denote the Gaussian prior on the parameters including the hidden layer weights and the readout weights.

To perform the integration over  $\mathbf{a}_\tau^\alpha$ , we use Hubbard-Stratonovich (H.S.) transformation and introduce a new vector field  $v_\tau^\alpha \in \mathbb{R}^P$

$$\begin{aligned} \mathcal{M}[\ell] &= \lim_{n \rightarrow 0} \prod_{\alpha=1}^n \prod_{\tau=1}^{\infty} \int d\Theta_\tau^\alpha \int dv_\tau^\alpha \int d\Theta_0 \\ &\exp \left( -\frac{i\beta}{2} \sum_{\tau=1}^{\infty} \sum_{\alpha=1}^n \left( \frac{1}{\sqrt{N_L}} f_{\text{train}}(\Theta_\tau^\alpha) - Y \right)^\top v_\tau^\alpha - \frac{\beta}{4} \sum_{\tau=1}^{\infty} \sum_{\alpha=1}^n |v_\tau^\alpha|^2 + \sum_{t=1}^{\infty} \sum_{\mathbf{x}} \ell_{t,\mathbf{x}} f(\mathbf{x}, \Theta_t^n) - S_0[\Theta] \right) \end{aligned} \quad (\text{B6})$$

**Averaging over the readout weights:**

We integrate over  $\mathbf{a}_\tau^\alpha$ . For convenience, we denote the set of all hidden layer weights collectively as  $\mathbf{W}_t = \{\mathbf{W}_t^{\ell=1}, \dots, \mathbf{W}_t^L\}$ , similar to the main text.

$$\mathcal{M}[\ell] = \lim_{n \rightarrow 0} \prod_{\tau=1}^{\infty} \prod_{\alpha=1}^n \int dv_\tau^\alpha \int d\mathbf{W}_\tau^\alpha \exp(-S[v, \mathbf{W}] - Q[\ell, v, \mathbf{W}] - S_0[\mathbf{W}]) \quad (\text{B7})$$

$$S[v, \mathbf{W}] = \frac{\beta}{4} \left( \sum_{\alpha, \beta=1}^n \sum_{\tau=1}^{\infty} \frac{\beta}{2} v_\tau^{\alpha\top} m_{\tau, \tau'}^{\alpha\beta} K_{\tau, \tau'}^{L, \alpha\beta}(\mathbf{W}_\tau^\alpha) v_{\tau'}^\beta + \sum_{\alpha=1}^n \sum_{\tau=1}^{\infty} (v_\tau^\alpha - 2iY)^\top v_\tau^\alpha \right) \quad (\text{B8})$$

and the source term action

$$Q[\ell, v, \mathbf{W}] = i\frac{\beta}{2} \sum_{\alpha=1}^n \sum_{t, \tau=1}^{\infty} \sum_{\mathbf{x}} v_\tau^{\alpha\top} m_{t, \tau}^{\alpha n} k_{t, \tau}^{L, \alpha n}(\mathbf{W}_\tau^\alpha, \mathbf{x}) \ell_{t, \mathbf{x}} - \frac{1}{2} \sum_{t, t'=1}^{\infty} \sum_{\mathbf{x}, \mathbf{x}'} m_{t, t'}^{nn} K_{t, t'}^{L, nn}(\mathbf{W}_\tau^n, \mathbf{x}, \mathbf{x}') \ell_{t, \mathbf{x}} \ell_{t', \mathbf{x}'} \quad (\text{B9})$$

Where  $m_{\tau, \tau'}^{\alpha\beta}$  is a scalar function independent of the data, and represents the averaging w.r.t. to the replica dependent prior  $S_0[\Theta]$ , such that  $\left\langle (\Theta_\tau^\alpha)_i (\Theta_{\tau'}^\beta)_j \right\rangle_{S_0} = \delta_{ij} m_{\tau, \tau'}^{\alpha\beta}$

$$m_{\tau, \tau'}^{\alpha\beta} = \begin{cases} m_{\tau, \tau'}^1 = \tilde{\sigma}^2 \left( \tilde{\lambda}^{|\tau-\tau'|} + \gamma \tilde{\lambda}^{\tau+\tau'} \right) & \{\alpha = \beta, \tau = \tau'\} \cup \{\alpha = n, \tau < \tau'\} \cup \{\beta = n, \tau > \tau'\} \\ m_{\tau, \tau'}^0 = \tilde{\sigma}^2 \left( \tilde{\lambda}^2 \tilde{\lambda}^{|\tau-\tau'|} + \gamma \tilde{\lambda}^{\tau+\tau'} \right) & \text{otherwise} \end{cases} \quad (\text{B10})$$

Where we have defined new functions of the parameters for convenience,

$$\tilde{\lambda} = \frac{\lambda}{\lambda + T\sigma^{-2}}, \tilde{\sigma}^2 = \sigma^2 \frac{\lambda + T\sigma^{-2}}{\lambda + \frac{1}{2}T\sigma^{-2}}, \gamma = \frac{\sigma_0^2}{\tilde{\sigma}^2} - 1 \quad (\text{B11})$$

The time-dependent and replica-dependent kernels  $K_{\tau, \tau'}^{L, \alpha\beta} \in \mathbb{R}^{P \times P}$ ,  $k_{\tau, \tau'}^{L, \alpha\beta}(\mathbf{x}) \in \mathbb{R}^P$ ,  $K_{\tau, \tau'}^{L, \alpha\beta}(\mathbf{x}, \mathbf{x}') \in \mathbb{R}^{P \times P}$  defined as:

$$\mathcal{K}_{\tau, \tau'}^{L, \alpha\beta}(\mathbf{x}, \mathbf{x}') = \frac{1}{N_L} \left( \mathbf{x}_\tau^L(\mathbf{x}, \mathbf{W}_\tau^\alpha) \cdot \mathbf{x}_{\tau'}^L(\mathbf{x}', \mathbf{W}_{\tau'}^\beta) \right) \quad (\text{B12})$$

And  $K_{\tau, \tau'}^{L, \alpha\beta} \in \mathbb{R}^{P \times P}$ ,  $k_{\tau, \tau'}^{L, \alpha\beta}(\mathbf{x}) \in \mathbb{R}^P$  are given by applying the kernel function on the training data and test data, respectively.

**Averaging over the hidden layer weights:**

In the infinite width limit, the statistics of  $\mathbf{W}_\tau^\alpha$  is dominated by its Gaussian prior (Eq.B5) with zero mean and covariance  $\langle \mathbf{W}_\tau^\alpha \mathbf{W}_{\tau'}^{\beta\top} \rangle = m_{\tau, \tau'}^{\alpha\beta} I$ . Thus the averaged kernel function  $K_{\tau, \tau'}^{\alpha\beta}$  (Eq.B12) over the prior yields two kinds of statistics for a given pair of times  $\{\tau, \tau'\}$ , which we denote as  $\mathcal{K}_{\tau, \tau'}^{1, L}(\mathbf{x}, \mathbf{x}')$ , and  $\mathcal{K}_{\tau, \tau'}^{0, L}(\mathbf{x}, \mathbf{x}')$ :

$$\mathcal{K}_{\tau, \tau'}^{\alpha\beta} = \begin{cases} \mathcal{K}_{\tau, \tau'}^1 & \{\alpha = \beta, \tau = \tau'\} \cup \{\alpha = n, \tau < \tau'\} \cup \{\beta = n, \tau > \tau'\} \\ \mathcal{K}_{\tau, \tau'}^0 & \text{otherwise} \end{cases} \quad (\text{B13})$$

And they obey the iterative relations:

$$\mathcal{K}_{\tau, \tau'}^{1, L}(\mathbf{x}, \mathbf{x}') = F \left( m_{\tau, \tau}^1 \mathcal{K}_{\tau, \tau}^{1, L-1}(\mathbf{x}, \mathbf{x}), m_{\tau', \tau'}^1 \mathcal{K}_{\tau', \tau'}^{1, L-1}(\mathbf{x}', \mathbf{x}'), m_{\tau, \tau'}^1 \mathcal{K}_{\tau, \tau'}^{1, L-1}(\mathbf{x}, \mathbf{x}') \right) \quad (\text{B14})$$

$$\mathcal{K}_{\tau,\tau'}^{0,L}(\mathbf{x}, \mathbf{x}') = F\left(m_{\tau,\tau}^1 \mathcal{K}_{\tau,\tau}^{1,L-1}(\mathbf{x}, \mathbf{x}), m_{\tau',\tau'}^1 \mathcal{K}_{\tau',\tau'}^{1,L-1}(\mathbf{x}', \mathbf{x}'), m_{\tau,\tau'}^0 \mathcal{K}_{\tau,\tau'}^{0,L-1}(\mathbf{x}, \mathbf{x}')\right) \quad (\text{B15})$$

$$\mathcal{K}^{1,L=0}(\mathbf{x}, \mathbf{x}') = \mathcal{K}^{0,L=0}(\mathbf{x}, \mathbf{x}') = \mathcal{K}^{in}(\mathbf{x}, \mathbf{x}') \quad (\text{B16})$$

$$\mathcal{K}^{in}(\mathbf{x}, \mathbf{x}') = \frac{1}{N_0} \sum_{i=1}^{N_0} \mathbf{x}_i \mathbf{x}'_i \quad (\text{B17})$$

where  $F(\langle z^2 \rangle, \langle z'^2 \rangle, \langle zz' \rangle)$  is a nonlinear function of the variances of two Gaussian variables  $z$  and  $z'$  and their covariance, whose form depends on the nonlinearity of the network [15]. As we see in Eqs.B14,B15 these variances and covariances depend on the kernel functions of the previous layer and on the replica-dependent prior statistics represented by  $m_{\tau,\tau'}^{1,0}$ .

The MGF can be written as a function of the statistics of one of these kernels, and their difference, which we will denote as  $\Delta_{\tau,\tau'}^L(\mathbf{x}, \mathbf{x}') = \frac{\lambda\beta}{2} \left( \mathcal{K}_{\tau,\tau'}^{1,L}(\mathbf{x}, \mathbf{x}') - \mathcal{K}_{\tau,\tau'}^{0,L}(\mathbf{x}, \mathbf{x}') \right)$ . It is useful to define a new kernel, the discrete neural dynamical kernel  $K_{\tau,\tau'}^{d,L} = \lim_{n \rightarrow 0} \frac{\lambda\beta}{2} \sum_{\alpha=1}^n m_{\tau,\tau'}^{n\beta} K_{\tau,\tau'}^{n\beta,L}$ , which controls the dynamics of the mean predictor. It has a simple expression in terms of the kernel  $\mathcal{K}_{\tau,\tau'}^{0,L}(\mathbf{x}, \mathbf{x}')$  and the kernel difference  $\Delta_{\tau,\tau'}^L$ .

$$\mathcal{K}_{\tau,\tau'}^{d,L}(\mathbf{x}, \mathbf{x}') = \begin{cases} 0 & \tau \leq \tau' \\ m_{\tau,\tau'}^1 \Delta_{\tau,\tau'}^L(\mathbf{x}, \mathbf{x}') + \tilde{\lambda}^{|\tau-\tau'|+1} \mathcal{K}_{\tau,\tau'}^{0,L}(\mathbf{x}, \mathbf{x}') & \tau > \tau' \end{cases} \quad (\text{B18})$$

We integrate over the replicated hidden layers variables  $\mathbf{W}_\tau^\alpha$ , which replaces the  $\mathbf{W}_\tau^\alpha$  dependent kernels with the averaged kernels. We thus get an MGF that depends only of the  $v_\tau^\alpha$  variables

$$\mathcal{M}[\ell] = \lim_{n \rightarrow 0} \prod_{\alpha=1}^n \prod_{\tau=1}^\infty \int dv_\tau^\alpha \exp(-S[v] - Q[\ell, v]) \quad (\text{B19})$$

$$S[v] = \frac{\beta}{4} \sum_{\tau=1}^\infty \left( \frac{\beta}{2} \sum_{\alpha,\beta=1}^n \sum_{\tau'=1}^\infty v_\tau^{\alpha\top} m_{\tau,\tau'}^0 K_{\tau,\tau'}^0 v_{\tau'}^\beta + \frac{2}{\lambda} \sum_{\alpha=1}^n \sum_{\tau'=1}^{t-1} v_\tau^{\alpha\top} K_{\tau,\tau'}^d v_{\tau'}^n \right. \\ \left. + \frac{1}{\lambda} \sum_{\alpha=1}^n v_\tau^{\alpha\top} K_{\tau,\tau}^d v_\tau^\alpha + \sum_{\alpha=1}^n v_\tau^{\alpha\top} (v_\tau^\alpha - 2iY) \right) \quad (\text{B20})$$

$$Q[\ell, v] = \frac{i\beta}{2} \sum_{\beta=1}^n \sum_{t,\tau'=1}^\infty \sum_{\mathbf{x}} \ell_{t,\mathbf{x}} m_{t,\tau'}^0 k_{t,\tau'}^{0\top}(\mathbf{x}) v_{\tau'}^\beta + \frac{i}{\lambda} \sum_{t,\tau'=1}^t \sum_{\mathbf{x}} \ell_{t,\mathbf{x}} k_{t,\tau'}^{d\top}(\mathbf{x}) v_{\tau'}^n \\ + \frac{i}{\lambda} \sum_{\beta=1}^n \sum_{t=1}^\infty \sum_{\tau'=t+1}^\infty \sum_{\mathbf{x}} \ell_{t,\mathbf{x}} k_{t,\tau'}^{d\top}(\mathbf{x}) v_{\tau'}^\beta - \sum_{t=1}^\infty \sum_{\mathbf{x}, \mathbf{x}'} \frac{1}{2} m_{t,t'}^1 \ell_{t,\mathbf{x}} \ell_{t',\mathbf{x}'} \mathcal{K}_{t,t'}^1(\mathbf{x}, \mathbf{x}') \quad (\text{B21})$$

## 2. Integrate Out Replicated Variables $v_\tau^\alpha$

We define a new variable  $u_\tau = \frac{\lambda\beta}{2} \sum_{\alpha=1}^n v_\tau^\alpha$ , and integrate out  $v_\tau^{\alpha \neq n}$ . We obtain a simpler expression of the MGF which is no longer replica dependent (after taking the limit  $n \rightarrow 0$ ).

$$\mathcal{M}[\ell] = \prod_{\tau=1}^\infty \int dv_\tau \int du_\tau \exp(-S[v, u] - Q[\ell, v, u]) \quad (\text{B22})$$

$$S[v, u] = \frac{1}{2\lambda^2} \sum_{\tau,\tau'=1}^\infty u_\tau^\top \left( m_{\tau,\tau'}^0 K_{\tau,\tau'}^0 - \frac{2}{\beta} \delta_{\tau,\tau'} \left( I + \frac{1}{\lambda} K_{\tau,\tau}^d \right) \right) u_{\tau'} \\ + \frac{1}{\lambda} \sum_{\tau=1}^\infty \left( \frac{1}{\lambda} \sum_{\tau'=1}^{\tau-1} K_{\tau,\tau'}^d v_{\tau'} + \left( I + \frac{1}{\lambda} K_{\tau,\tau}^d \right) v_\tau - iY \right)^\top u_\tau \quad (\text{B23})$$

$$\begin{aligned}
Q[\ell, v, u] = & \frac{i}{\lambda} \sum_{t=1}^{\infty} \sum_{\mathbf{x}} \ell_{t,\mathbf{x}} \left( \sum_{\tau'=1}^{\infty} m_{t,\tau'}^0 k_{t,\tau'}^{0\top} u_{\tau'} + \sum_{\tau'=1}^t k_{t,\tau'}^{d\top} v_{\tau'} + \frac{2}{\lambda\beta} \sum_{\tau'=t+1}^{\infty} k_{t,\tau'}^{d\top} u_{\tau'} \right) \\
& - \sum_{t,t'=1}^{\infty} \sum_{\mathbf{x},\mathbf{x}'} \frac{1}{2} \ell_{t,\mathbf{x}} \ell_{t',\mathbf{x}'} m_{t,t'}^1 k_{t,t'}^1(\mathbf{x}, \mathbf{x}')
\end{aligned} \tag{B24}$$

### 3. Detailed Calculation of the Mean Predictor

To derive the mean predictor we take the derivative of the MGF w.r.t.  $\ell_{t,\mathbf{x}}$ :

$$\langle f(t, \mathbf{x}) \rangle = \left. \frac{\partial \mathcal{M}[\ell]}{\partial \ell_{t,\mathbf{x}}} \right|_{\ell_{t,\mathbf{x}}=0} \tag{B25}$$

which yields

$$\langle f(t, \mathbf{x}) \rangle = \frac{1}{\lambda} \sum_{t'=1}^t k_{t,t'}^{d,L\top}(\mathbf{x}) \langle -iv_{t'} \rangle \tag{B26}$$

Furthermore, from the H.S. transformation in Eq.B6, we can relate  $\langle v_{\tau} \rangle$  to the mean predictor on the training data  $f_{\text{train}}(t)$

$$iv_t = f_{\text{train}}(t) - Y \tag{B27}$$

For all moments of  $f_{\text{train}}(t)$ . On the other hand we can get the statistics of  $iv_t$  from the MGF in Eq.B22.

$$\langle f_{\text{train}}(t) \rangle = \left( I\lambda + K_{t,t}^{d,L} \right)^{-1} \sum_{t'=1}^{t-1} K_{t,t'}^{d,L} (Y - \langle f_{\text{train}}(t') \rangle) \tag{B28}$$

$$\langle f(t, \mathbf{x}) \rangle = \frac{1}{\lambda} \sum_{t'=1}^t k_{t,t'}^{d,L\top}(\mathbf{x}) (Y - \langle (f_{\text{train}})_{t'} \rangle) \tag{B29}$$

where  $K_{t,t'}^{d,L}$  is a  $P \times P$  dimensional kernel matrix defined as  $K_{\mu\nu,t,t'}^{d,L} = K_{t,t'}^{d,L}(\mathbf{x}^\mu, \mathbf{x}^\nu)$ . Now we can compute  $\langle f(\mathbf{x}, \Theta_t) \rangle$  iteratively by combining Eqs.B28,B29.

### 4. Large $\lambda$ Limit

All the results so far hold for any  $T$  and  $\lambda$ . Now, we consider the limit where the Markov proximal learning algorithm is equivalent to Langevin dynamics in order to get expressions that are relevant to a continuous time gradient descent. We consider  $\lambda \rightarrow \infty$  and  $t_{\text{discrete}} \sim O(\lambda)$ , and thus define a new continuous time  $t = t_{\text{discrete}}/\lambda \sim O(1)$ . In this limit, the parameters defined in Eq.B11 becomes

$$\tilde{\lambda}^{t_{\text{discrete}}} = e^{-T\sigma^{-2}t}, \tilde{\sigma}^2 = \sigma^2, \gamma = \frac{\sigma_0^2}{\sigma^2} - 1 \tag{B30}$$

Taking the limit of large  $\lambda$  limit of Eq.B22 is straightforward, and yields

$$\mathcal{M}[\ell] = \int Dv \int Du \exp(-S[v, u] - Q[\ell, v, u]) \tag{B31}$$

Where

$$\begin{aligned}
S[v, u] = & \frac{1}{2} \int_0^{\infty} dt \int_0^{\infty} dt' m(t, t') u^\top(t) K^L(t, t') u(t') \\
& + \int_0^{\infty} dt \left( \int_0^t dt' K_d^L(t, t') v(t') + v(t) - iY \right)^\top u(t)
\end{aligned} \tag{B32}$$

and the source term action is

$$\begin{aligned}
Q[\ell, v, u] = & i \int_0^\infty dt \int_0^t dt' (K_d^L(t, t'))^\top v(t') \ell(t) \\
& + i \int_0^\infty dt \int_0^\infty dt' m(t, t') (k^L(t, t'))^\top u(t') \ell(t) \\
& - \frac{1}{2} \int_0^\infty dt \int_0^\infty dt' m(t, t') k^L(t, t', \mathbf{x}, \mathbf{x}') \ell(t) \ell(t')
\end{aligned} \tag{B33}$$

Where in the infinite width limit, we can identify  $v(t)$  with  $f_{\text{train}}(t)$  by  $iv_t = f_{\text{train}}(t) - Y$ , which holds for all moments of  $f_{\text{train}}(t)$ , and thus to write the MGF in terms of  $f_{\text{train}}(t)$ , as was done in the main text Eqs.10, 11, 12.

For convenience, in the continuous time limit, we denote the NDK with a lower index  $d$ . The NDK in Eq.B18 can be rewritten as

$$\mathcal{K}_d^L(t, t', \mathbf{x}, \mathbf{x}') = m(t, t') \Delta^L(t, t', \mathbf{x}, \mathbf{x}') + e^{-T\sigma^{-2}|t-t'|} \mathcal{K}^L(t, t', \mathbf{x}, \mathbf{x}') \tag{B34}$$

with

$$\begin{aligned}
\Delta^L(t, t', \mathbf{x}, \mathbf{x}') &= \frac{\lambda}{2T} (\mathcal{K}^{L,1}(t, t', \mathbf{x}, \mathbf{x}') - \mathcal{K}^{L,0}(t, t', \mathbf{x}, \mathbf{x}')) \\
&= \mathcal{K}^{d,L-1}(t, t', \mathbf{x}, \mathbf{x}') \dot{\mathcal{K}}^L(t, t', \mathbf{x}, \mathbf{x}')
\end{aligned} \tag{B35}$$

$$m(t, t') = \sigma^2 e^{-T\sigma^{-2}|t-t'|} + (\sigma_0^2 - \sigma^2) e^{-T\sigma^{-2}(t+t')} \tag{B36}$$

With the kernels defined in Sec.IV in the main text. Here the quantity  $m(t, t')$  is the continuous time limit of  $m_{t,t'}^1$ . As defined in Eq.B10, it represents the covariance of the prior

$$\langle \Theta_t^i \Theta_{t'}^j \rangle_{S_0} = \delta_{ij} m(t, t'), \langle \Theta_t^i \rangle_{S_0} = 0 \tag{B37}$$

The above calculation leads to the recursion relation of  $\mathcal{K}_d^L(t, t', \mathbf{x}, \mathbf{x}')$  given in Eq.17 in the main text:

$$\begin{aligned}
\mathcal{K}_d^L(t, t', \mathbf{x}, \mathbf{x}') &= m(t, t') \mathcal{K}_d^{L-1}(t, t', \mathbf{x}, \mathbf{x}') \dot{\mathcal{K}}^L(t, t', \mathbf{x}, \mathbf{x}') \\
&+ e^{-T\sigma^{-2}|t-t'|} \mathcal{K}^L(t, t', \mathbf{x}, \mathbf{x}')
\end{aligned} \tag{B38}$$

with initial condition

$$\mathcal{K}_d^{L=0}(t, t', \mathbf{x}, \mathbf{x}') = e^{-T\sigma^{-2}|t-t'|} \mathcal{K}_{in}(\mathbf{x}, \mathbf{x}') \tag{B39}$$

Where  $\mathcal{K}_{in}(\mathbf{x}, \mathbf{x}')$  was defined in Eq.B17. We refer to this continuous time  $\mathcal{K}_d^L(t, t', \mathbf{x}, \mathbf{x}')$  as the Neural Dynamical Kernel (NDK). Note that it follows directly from Eq.17 that

$$\mathcal{K}_d^L(0, 0, \mathbf{x}, \mathbf{x}') = \mathcal{K}_{NTK}^L(\mathbf{x}, \mathbf{x}'). \tag{B40}$$

For the mean predictor we use the results from the previous section Eqs.B27,B28,B29, take the large  $\lambda$  limit and turn the sums into integrals, we obtain

$$\langle f_{\text{train}}(t) \rangle = \int_0^t dt' K_d^L(t, t') (Y - \langle f_{\text{train}}(t') \rangle) \tag{B41}$$

$$\langle f(t, \mathbf{x}) \rangle = \int_0^t dt' (k_d^L(t, t', \mathbf{x}))^\top (Y - \langle f_{\text{train}}(t') \rangle) \tag{B42}$$

as given in Eqs.20, 21 in the main text.

## 5. Low $T$ limit

We aim to formally take the limit  $T \rightarrow 0$  of Eqs. B41, B42. In this limit, it is natural to rescale the times  $t_{scaled} = (T\sigma^{-2})t$ , and consider  $t_{scaled} \sim \mathcal{O}(1)$ , which accounts for the diffusive learning phase, where  $t \sim \mathcal{O}(1/T)$ . For convenience, we will drop the "scaled" and consider this subsection purely in scaled time. We first look at the leading contribution of the gradient-driven phase described by the NTK.

$$\lim_{T \rightarrow 0} \langle f_{train}(t) \rangle = \lim_{T \rightarrow 0} \left( \left( I - \exp \left( -\frac{\sigma^2}{T} K_{NTK}^L t \right) \right) Y \right) = Y - T\sigma^{-2} \delta(t) (K_{NTK}^L)^{-1} Y \quad (\text{B43})$$

We expand  $\langle f_{train}(t) \rangle$  around  $Y$  to leading correction in  $T$

$$\langle f_{train}(t) \rangle \approx Y - T\sigma^{-2} (\delta(t) K_{NTK}^{-1} Y + f_1(t)) \quad (\text{B44})$$

Using Eqs.B41, B42, we find the integral equation for  $f_1(t)$

$$\int_0^t dt' K_d^L(t, t') f_1(t') = (I - K_d^L(t, 0) K_{NTK}^{-1}) Y \quad (\text{B45})$$

And the equation for  $\langle f(t, \mathbf{x}) \rangle$  in terms of  $f_1(t)$

$$\langle f(t, \mathbf{x}) \rangle = k_d^L(t, 0)^\top (K_{NTK}^L)^{-1} Y + \int_0^t dt' k_d^L(t, t', \mathbf{x})^\top f_1(t') \quad (\text{B46})$$

At  $t = 0$ ,  $\langle f(\mathbf{x}, 0) \rangle = (k_{NTK}^L)^\top (K_{NTK}^L)^{-1} Y$ , which is the NTK equilibrium, marks the transition to the diffusive learning phase. At long time, looking for a constant solution to Eq.B46, and using the identity in Eq.16 we find the equilibrium

$$\lim_{t \rightarrow \infty} \langle f(t, \mathbf{x}) \rangle = k_{GP}^\top (K_{GP}^L)^{-1} Y \quad (\text{B47})$$

Which is the NNGP equilibrium when taking  $T \rightarrow 0$ .

## Appendix C: Second Moment

Our formalism allows for the derivation of higher moments of the predictor. In particular, we are interested in the covariance  $\langle \delta f(t, \mathbf{x}) \delta f(t', \mathbf{x}') \rangle \equiv \langle f(t, \mathbf{x}) f(t', \mathbf{x}') \rangle - \langle f(t, \mathbf{x}) \rangle \langle f(t', \mathbf{x}') \rangle$ . We focus on the continuous time  $\lambda \rightarrow \infty$  limit described in Sec.B4, which is equivalent to Langevin dynamics. In order to calculate the second moment, we need to invert one time-dependent operator, which we denote as  $B(t, t') \in \mathbb{R}^{P \times P}$ :

$$B(t, t') = I \delta(t - t') + K_d^L(t, t'), \quad (\text{C1})$$

$$\int_0^t d\tau B(t, \tau) B^{-1}(\tau, t') = I \delta(t - t') \quad (\text{C2})$$

The full statistics of the Gaussian field  $v(t), u(t)$  can be written in terms of  $B^{-1}(t, t')$

$$\langle v(t) \rangle = i \int_0^t dt' B^{-1}(t, t') Y \quad (\text{C3})$$

$$\langle \delta v(t) \delta v^\top(t') \rangle = - \int_0^\infty d\tau' \int_0^\infty d\tau B^{-1}(t, \tau) m(\tau, \tau') K^L(\tau, \tau') B^{-1}(t', \tau') \quad (\text{C4})$$

$$\langle v(t) u^\top(t') \rangle = B^{-1}(t, t') \quad (\text{C5})$$

It is useful to separate the smooth part from the delta function in the inverse operator  $B^{-1}(t, t')$ . We denote the smooth function as  $J(t, t') \in \mathbb{R}^{P \times P}$ , which satisfies the following integral equation:

$$J(t, t') = \begin{cases} K_d^L(t, t') - \int_{t'}^t d\tau K_d^L(t, \tau) J(\tau, t') & t \geq t' \\ 0 & t < t' \end{cases} \quad (\text{C6})$$

$$B^{-1}(t, t') = I\delta(t - t') - J(t, t') \quad (\text{C7})$$

We take the second derivative of the MGF (Eq.B31):

$$\langle \delta f(\mathbf{x}, t) \delta f(\mathbf{x}', t') \rangle = \frac{\partial^2 \mathcal{M}[\ell]}{\partial \ell(t, \mathbf{x}) \partial \ell(t', \mathbf{x}')} \Big|_{\ell(t, \mathbf{x}) = \ell(t', \mathbf{x}') = 0} - \langle f(\mathbf{x}, t) \rangle \langle f(\mathbf{x}', t') \rangle \quad (\text{C8})$$

Which we can express in terms of  $J(t, t')$  using the derived statistics of  $v(t), u(t)$

$$\begin{aligned} \langle \delta f_{\text{train}}(t) \delta f_{\text{train}}^\top(t') \rangle &= m(t, t') K^L(t, t') - \int_0^t d\tau [J(t, \tau) m(t', \tau) K^L(t', \tau)] \\ &\quad - \int_0^{t'} d\tau [J(t', \tau) m(t, \tau) K^L(t, \tau)] + \int_0^t d\tau \int_0^{t'} d\tau' [J(t, \tau) m(\tau, \tau') K^L(\tau, \tau') J(t', \tau')] \end{aligned} \quad (\text{C9})$$

$$\begin{aligned} \langle \delta f(t, \mathbf{x}) \delta f(t', \mathbf{x}') \rangle &= \int_0^t d\tau \int_0^{t'} d\tau' [k_d^L(t, \tau, \mathbf{x})^\top \langle \delta f_{\text{train}}(\tau) \delta f_{\text{train}}^\top(\tau') \rangle k_d^L(t', \tau', \mathbf{x}')] \\ &\quad + \int_0^t d\tau \int_0^\tau d\tau' [k_d^L(t, \tau, \mathbf{x})^\top J(\tau, \tau') m(t', \tau') k^L(t', \tau', \mathbf{x}')] + \int_0^{t'} d\tau \int_0^\tau d\tau' [m(t, \tau) k^L(t, \tau, \mathbf{x})^\top J(\tau, \tau') k_d^L(t', \tau', \mathbf{x}')] \\ &\quad - \int_0^t d\tau [k_d^L(t, \tau, \mathbf{x})^\top m(t', \tau) k^L(t', \tau, \mathbf{x}')] - \int_0^{t'} d\tau [m(t, \tau) k^L(t, \tau, \mathbf{x})^\top k_d^L(t', \tau, \mathbf{x}')] + m(t, t') \mathcal{K}^L(t, t', \mathbf{x}, \mathbf{x}') \end{aligned} \quad (\text{C10})$$

The equation becomes simpler for the correlation with initial condition, achieved by plugging  $t' = 0$  in Eq.C10

$$\begin{aligned} \langle \delta f(t, \mathbf{x}) \delta f(t' = 0, \mathbf{x}') \rangle &= m(t, 0) \mathcal{K}^L(t, 0, \mathbf{x}, \mathbf{x}') - \int_0^t d\tau [k_d^L(t, \tau, \mathbf{x})^\top m(\tau, 0) k^L(\tau, 0, \mathbf{x}')] \\ &\quad + \int_0^t d\tau \int_0^\tau d\tau' [k_d^L(t, \tau, \mathbf{x})^\top J(\tau, \tau') m(\tau', 0) k^L(\tau', 0, \mathbf{x}')] \end{aligned} \quad (\text{C11})$$

We note that the mean predictor can also be written using the  $J(t, t')$  operator:

$$\langle f_{\text{train}}(t) \rangle = \int_0^t dt' J(t, t') Y \quad (\text{C12})$$

$$\langle f(t, \mathbf{x}) \rangle = \int_0^t dt' \left[ k_d^L(t, t', \mathbf{x})^\top \left( I - \int_0^{t'} dt'' J(t', t'') \right) \right] Y \quad (\text{C13})$$

Solving the integral equation for  $J(t, t')$  for a general nonlinearity is complex. However, the equations are tractable in two cases: Linear networks and the NTK limit ( $T \rightarrow 0, t \sim \mathcal{O}(1)$ ), which are presented below.

## 1. The NTK Limit

The time dependence of all kernels arises from  $m(t, t')$ , and thus at the NTK limit, defined by  $T \rightarrow 0, t \sim \mathcal{O}(1)$ , we can substitute all the kernels and temporal correlations with their values at initialization, specifically  $K_d^L(t, t') \approx K_{NTK}^L, K(t, t') = K_{GP_0}, m(t, t') = \sigma_0^2$ . Solving  $J(t, t')$  with a constant NDK yields

$$J(t, t') = \begin{cases} K_{NTK}^L \exp(-K_{NTK}^L (t - t')) & t \geq t' \\ 0 & t < t' \end{cases} \quad (\text{C14})$$

The only time dependence in the covariance equation (Eq.C10) comes from  $J(t, t')$ , as the kernels and  $m(t, t')$  are constant. Performing the integral over the exponential  $J(t, t')$  results in

$$\begin{aligned} \lim_{T \rightarrow 0} \sigma_0^{-2} \langle \delta f(t, \mathbf{x}) \delta f(t', \mathbf{x}') \rangle &= \mathcal{K}_{GP_0}^L(\mathbf{x}, \mathbf{x}') - k_{GP_0}^L(\mathbf{x}) (K_{GP_0}^L)^{-1} k_{GP_0}^L(\mathbf{x}') \\ &+ \left[ (I - \exp(-K_{NTK}^L t)) (K_{NTK}^L)^{-1} k_{NTK}^L(\mathbf{x}) - (K_{GP_0}^L)^{-1} k_{GP_0}^L(\mathbf{x}) \right]^\top K_{GP_0}^L \\ &\cdot \left[ (I - \exp(-K_{NTK}^L t')) (K_{NTK}^L)^{-1} k_{NTK}^L(\mathbf{x}') - (K_{GP_0}^L)^{-1} k_{GP_0}^L(\mathbf{x}') \right] \end{aligned} \quad (\text{C15})$$

Which is the result from Sec.V A.

## 2. Linear Network

For a linear network, the NDK can be written in terms of the sum of exponents (see Sec.E), and the integral equations for the first and second moments are tractable. We can represent both of them in terms of the function  $J(t, t')$  (Eq.C6)

$$\begin{aligned} J(t, t') &= K_d^L(t', t') \\ \exp \left( - (L + 1) \left( (K_{GP}^L + IT\sigma^{-2})(t - t') + \frac{1}{2T\sigma^{-2}} K_{GP}^L \sum_{n=1}^L \frac{L!}{n! (L-n)!} \frac{\gamma^n}{n} \left( e^{-2T\sigma^{-2}nt'} - e^{-2T\sigma^{-2}nt} \right) \right) \right) \end{aligned} \quad (\text{C16})$$

Where  $K_{GP}^L = \sigma^{2L} K_{in}$ ,  $K_{in}$  is defined in Eq.B17 and  $K_d^L(t, t')$  is given in linear network in Eq.E4.

The mean predictor and the covariance can be calculated by substituting the expression for  $J(t, t')$  into Eqs.C10, C13, leading to integrals that can be evaluated numerically, rather than integral equations like in the nonlinear case.

### Low $T$ Limit:

We can further simplify the expressions by taking the limit of  $T \rightarrow 0$ . In this limit,  $J(t, t')$  is singular around  $t = t'$  and is given by

$$J(t, t') = T\sigma^{-2} \left( I\delta(t - t') + T\sigma^{-2} (K_d^L(t, t))^{-1} (\delta'(t - t') + (L + 1)\delta(t - t')) \right) \quad (\text{C17})$$

Where  $\delta(t - t')$  and  $\delta'(t - t')$  are the Dirac delta function and its derivative, respectively. The leading order in  $T$  of the mean predictor is

$$f(t, \mathbf{x}) = k_{in}(\mathbf{x})^\top K_{in}^{-1} (I - \exp(-(L + 1)\sigma_0^{2L} K_{in} t)) Y \quad (\text{C18})$$

It is important to note that in a linear network, the NTK equilibrium identifies with the NNGP equilibrium, and thus, the mean predictor dynamics are identical to the NTK dynamics, and reaches equilibrium at  $t \sim \mathcal{O}(1)$ .

The covariance equation in the low  $T$  limit take the following simple form

$$\langle \delta f(t, \mathbf{x}) \delta f(t', \mathbf{x}') \rangle = m^{L+1}(t, t') \left[ \mathcal{K}_{in}(\mathbf{x}, \mathbf{x}') - k_{in}(\mathbf{x})^\top (K_{in})^{-1} k_{in}(\mathbf{x}') \right]$$

The covariance can exhibit non-trivial dynamics at the diffusive phase, depending on the values of  $\sigma, \sigma_0$ , as shown in Fig.4.

## Appendix D: Multiple Outputs

The derivation from SI Sec.B can be repeated in the case of multiple outputs. We denote the number of outputs as  $m$ , and the predictor and target labels are  $m$ -dimensional vectors  $f(\mathbf{x}, t) \in \mathbb{R}^m$ ,  $y^\mu \in \mathbb{R}^m$ , and the readout is a matrix  $\mathbf{a}(t) \in \mathbb{R}^{N_L \times m}$ . As long as the prior is an elementwise norm of the parameters  $\Theta$ , the MGF breaks down to  $m$  uncoupled components, leading to the following mean field equations for the mean predictor:

$$\langle f_{\text{train}}(t) \rangle = \int_0^t dt' K_d^L(t, t') (Y - \langle f_{\text{train}}(t') \rangle) \quad (\text{D1})$$

Where  $f_{\text{train}}(t)$ ,  $Y \in \mathbb{R}^{P \times m}$  are matrices, and  $K_d^L(t, t') \in \mathbb{R}^{P \times P}$  is the NDK as defined in previous parts (Sec. IV). The equation for the predictor on a test point is given by

$$\langle f(t, \mathbf{x}) \rangle = \int_0^t dt' (Y - \langle f_{\text{train}}(t') \rangle)^\top k_d^L(t, t', \mathbf{x}) \quad (\text{D2})$$

Where  $k_d^L(t, t') \in \mathbb{R}^P$  is the NDK test vector as defined in previous parts (Sec. IV). The result is an  $m$ -dimensional vector  $f(t, \mathbf{x}) \in \mathbb{R}^m$  as required, and  $f_{\text{train}}^\mu(t) = f^\top(t, \mathbf{x}_\mu)$ .

Due to the uncoupling of the MGF, the covariance is diagonal in the outputs

$$\langle \delta f_m(t, \mathbf{x}) \delta f_{m'}(t', \mathbf{x}') \rangle \propto \delta_{m, m'} \quad (\text{D3})$$

Where for each output the covariance satisfies the same equations as described in SI Sec.C, and the covariance between different outputs is zero.

## Appendix E: The Neural Dynamical Kernel

We focus on the continuous time limit derived above, and present several examples where the NDK has explicit expressions, and provide proofs of properties of the NDK presented in the main text. We have derived

$$\begin{aligned} \mathcal{K}_d^L(t, t', \mathbf{x}, \mathbf{x}') &= m(t, t') \mathcal{K}_d^{L-1}(t, t', \mathbf{x}, \mathbf{x}') \dot{\mathcal{K}}^L(t, t', \mathbf{x}, \mathbf{x}') \\ &\quad + e^{-T\sigma^{-2}|t-t'|} \mathcal{K}^L(t, t', \mathbf{x}, \mathbf{x}') \end{aligned} \quad (\text{E1})$$

In order to complete the calculation of the NDK, we would provide explicit analytical expressions for  $\mathcal{K}(t, t', \mathbf{x}, \mathbf{x}')$  and  $\dot{\mathcal{K}}(t, t', \mathbf{x}, \mathbf{x}')$  in cases where they are available, namely linear activation, and ReLU and error function nonlinearities.

### 1. Linear Activation:

For linear activation:

$$\mathcal{K}^L(t, t', \mathbf{x}, \mathbf{x}') = (m(t, t'))^L \mathcal{K}_{in}(\mathbf{x}, \mathbf{x}') \quad (\text{E2})$$

$$\dot{\mathcal{K}}^L(t, t', \mathbf{x}, \mathbf{x}') = I \quad (\text{E3})$$

The recursion relation for the NDK can be solved explicitly, yielding

$$\mathcal{K}_d^L(t, t', \mathbf{x}, \mathbf{x}') = (m(t, t'))^L (L + 1) e^{-T\sigma^{-2}|t-t'|} \mathcal{K}_{in}(\mathbf{x}, \mathbf{x}') \quad (\text{E4})$$

The NDK of linear activation is proportional to the input kernel  $\mathcal{K}_{in}(\mathbf{x}, \mathbf{x}')$  regardless of the data. The effect of network depth only changes the magnitude but not the shape of the NDK. As a result, the NNGP and NTK kernels also only differ by their magnitude, and thus the mean predictor at the NNGP and NTK equilibria only differ by  $\mathcal{O}(T)$ . This suggests that the diffusive phase has very little effect on the mean predictor in the low  $T$  regime, in linear network, as discussed in Sec.C2.

## 2. ReLU Activation:

For ReLU activation, we define the function  $J(\theta)$  [15]:

$$J(\theta^L(t, t', \mathbf{x}, \mathbf{x}')) = (\pi - \theta^L(t, t', \mathbf{x}, \mathbf{x}')) \cos(\theta^L(t, t', \mathbf{x}, \mathbf{x}')) + \sin(\theta^L(t, t', \mathbf{x}, \mathbf{x}')) \quad (\text{E5})$$

where the angle between  $\mathbf{x}$  and  $\mathbf{x}'$  is given by :

$$\theta^L(t, t', \mathbf{x}, \mathbf{x}') = \cos^{-1} \left( \frac{m(t, t')}{\sqrt{m(t, t) m(t', t')}} \frac{1}{\pi} J(\theta^{L-1}(t, t', \mathbf{x}, \mathbf{x}')) \right) \quad (\text{E6})$$

$\theta^L(t, t', \mathbf{x}, \mathbf{x}')$  is defined through a recursion equation, and

$$\theta^{L=0}(t, t', \mathbf{x}, \mathbf{x}') = \cos^{-1} \left( \frac{m(t, t')}{\sqrt{m(t, t) m(t', t')}} \frac{\mathcal{K}_{in}(\mathbf{x}, \mathbf{x}')}{\sqrt{\mathcal{K}_{in}(\mathbf{x}, \mathbf{x}) \mathcal{K}_{in}(\mathbf{x}', \mathbf{x}')}} \right) \quad (\text{E7})$$

the kernel functions are then given by

$$\dot{\mathcal{K}}^L(t, t', \mathbf{x}, \mathbf{x}') = \frac{1}{2\pi} (\pi - \theta^L(t, t', \mathbf{x}, \mathbf{x}')) \quad (\text{E8})$$

$$\mathcal{K}^L(t, t', \mathbf{x}, \mathbf{x}') = \frac{\sqrt{\mathcal{K}_{in}(\mathbf{x}, \mathbf{x}) \mathcal{K}_{in}(\mathbf{x}', \mathbf{x}')}}{\pi 2^L} (m(t, t) m(t', t'))^{L/2} J(\theta^{L-1}(t, t', \mathbf{x}, \mathbf{x}')) \quad (\text{E9})$$

We obtain an explicit expression for the NDK by plugging these kernels into Eqs.17,B39.

## 3. Error Function Activation

For error function activation [10]:

$$\mathcal{K}^L(t, t', \mathbf{x}, \mathbf{x}') = \frac{2}{\pi} \sin^{-1} \left( \frac{2m(t, t') \mathcal{K}^{L-1}(t, t', \mathbf{x}, \mathbf{x}')}{\sqrt{(1 + 2m(t, t) \mathcal{K}^{L-1}(t, t, \mathbf{x}, \mathbf{x})) (1 + 2m(t', t') \mathcal{K}^{L-1}(t', t', \mathbf{x}', \mathbf{x}'))}} \right) \quad (\text{E10})$$

$$\begin{aligned} \dot{\mathcal{K}}_{\mu\nu}^L(t, t', \mathbf{x}, \mathbf{x}') &= \frac{4}{\pi} \left( (1 + 2m(t, t) \mathcal{K}^{L-1}(t, t, \mathbf{x}, \mathbf{x})) (1 + 2m(t', t') \mathcal{K}^{L-1}(t', t', \mathbf{x}', \mathbf{x}')) \right. \\ &\quad \left. - 4(m(t, t') \mathcal{K}^{L-1}(t, t', \mathbf{x}, \mathbf{x}'))^2 \right)^{-1/2} \end{aligned} \quad (\text{E11})$$

Again we can obtain an explicit expression for the NDK by plugging these kernels into Eqs.17,B39.

## 4. Long Time Behavior of the NDK

We define the long time limit as  $t, t' \rightarrow \infty, t - t' \sim \mathcal{O}(T^{-1})$ . At a long time the statistics of  $\mathbf{W}$  w.r.t. the prior becomes only a function of the time difference:

$$\langle \mathbf{W}_t \mathbf{W}_{t'}^\top \rangle = \sigma^2 e^{-T\sigma^{-2}|t-t'|} = m(|t-t'|) \quad (\text{E12})$$

And thus, the kernels defined above also will be only functions of the time difference. We look at the time derivative of the kernel (w.l.o.g. we assume  $t > t'$ ), which can be obtained with a chain rule:

$$\frac{d}{dt'} \mathcal{K}^L(t - t', \mathbf{x}, \mathbf{x}') = \dot{\mathcal{K}}^L(t - t', \mathbf{x}, \mathbf{x}') \frac{d}{dt'} (\mathcal{K}^{L-1}(t - t', \mathbf{x}, \mathbf{x}') m(t - t')) \quad (\text{E13})$$

We prove by induction:

$$\frac{1}{T} \frac{d}{dt'} (m(t-t') \mathcal{K}^L(t-t', \mathbf{x}, \mathbf{x}')) = \mathcal{K}_d^L(t-t', \mathbf{x}, \mathbf{x}') \quad (\text{E14})$$

The induction basis for  $L = 0$  is trivial. For arbitrary  $L + 1$ :

$$\begin{aligned} \frac{1}{T} \frac{d}{dt'} (m(t-t') \mathcal{K}^{L+1}(t-t', \mathbf{x}, \mathbf{x}')) &= m(t-t') \dot{\mathcal{K}}^{L+1}(t-t', \mathbf{x}, \mathbf{x}') \frac{1}{T} \frac{d}{dt'} (\mathcal{K}^L(t-t', \mathbf{x}, \mathbf{x}') m(t-t')) \\ &\quad + e^{-T\sigma^{-2}(t-t')} \mathcal{K}^{L+1}(t-t', \mathbf{x}, \mathbf{x}') \end{aligned} \quad (\text{E15})$$

And using the induction assumption we get:

$$\begin{aligned} \frac{1}{T} \frac{d}{dt'} (m(t-t') \mathcal{K}^{L+1}(t-t', \mathbf{x}, \mathbf{x}')) &= m(t-t') \dot{\mathcal{K}}^{L+1}(t-t', \mathbf{x}, \mathbf{x}') \mathcal{K}_d^L(t-t', \mathbf{x}, \mathbf{x}') \\ &\quad + e^{-T\sigma^{-2}(t-t')} \mathcal{K}^{L+1}(t-t', \mathbf{x}, \mathbf{x}') \end{aligned} \quad (\text{E16})$$

Which is the expression for  $\mathcal{K}^{d,L+1}(t-t')$ . Using this identity, we can get a simple expression for the integral over  $\mathcal{K}_d^L(t-t')$  at long times:

$$\lim_{t \rightarrow \infty} \left( \frac{T}{\sigma^2} \int_0^t dt' \mathcal{K}_d^L(t-t', \mathbf{x}, \mathbf{x}') \right) = \mathcal{K}_{GP}^L(\mathbf{x}, \mathbf{x}') \quad (\text{E17})$$

## 5. NDK as a Generalized Time-Dependent NTK

In Eq.14 in the main text, we claimed that the NDK has the following interpretation as a generalized two-time NTK

$$\mathcal{K}_d^L(t, t', \mathbf{x}, \mathbf{x}') = e^{-T\sigma^{-2}|t-t'|} \langle \nabla_{\Theta_t} f(\mathbf{x}, \Theta_t) \cdot \nabla_{\Theta_{t'}} f(\mathbf{x}', \Theta_{t'}) \rangle_0 \quad t \geq t' \quad (\text{E18})$$

where  $\langle \cdot \rangle_0$  denotes averaging w.r.t. the prior distribution of the parameters  $\Theta$ , with the statistics defined in Eq.7. Now we provide a formal proof.

We separate  $\nabla_{\Theta_t} f(\mathbf{x}, \Theta_t)$  into two parts including the derivative w.r.t. the readout weights  $a_t$  and the hidden layer weights  $\mathbf{W}_t$

**Derivative w.r.t. the readout weights:**

$$\langle \partial_{\mathbf{a}_t} f(\mathbf{x}, \Theta_t) \cdot \partial_{\mathbf{a}_{t'}} f(\mathbf{x}, \Theta_{t'}) \rangle_0 = \mathcal{K}^L(t, t', \mathbf{x}, \mathbf{x}') \quad (\text{E19})$$

**Derivative w.r.t. the hidden layer weights:**

We have

$$\partial_{\mathbf{W}_t^l} \mathbf{x}_t^L(\mathbf{x}, \mathbf{W}_t) = \frac{1}{\sqrt{N_{L-1} \cdots N_{l-1}}} \Pi_{k=l+1}^L [\phi'(z_t^k) \mathbf{W}_t^k] \phi'(z_t^l) \mathbf{x}_t^{l-1} \quad (\text{E20})$$

and

$$\begin{aligned} &\langle \partial_{\mathbf{W}_t^l} f(\mathbf{x}, \Theta_t) \cdot \partial_{\mathbf{W}_{t'}^l} f(\mathbf{x}, \Theta_{t'}) \rangle_0 \\ &= \langle N_L^{-1} \mathbf{a}_t \cdot \mathbf{a}_{t'} \rangle (\Pi_{k=l+1}^L \langle N_k^{-1} N_{k-1}^{-1} \mathbf{W}_t^k \cdot \mathbf{W}_{t'}^k \rangle) \left( \Pi_{k=l}^L \dot{\mathcal{K}}^k(t, t', \mathbf{x}, \mathbf{x}') \right) \mathcal{K}^{l-1}(t, t', \mathbf{x}, \mathbf{x}') \\ &= m(t, t')^{L-l+1} \left( \Pi_{k=l}^L \dot{\mathcal{K}}^k(t, t', \mathbf{x}, \mathbf{x}') \right) \mathcal{K}^{l-1}(t, t', \mathbf{x}, \mathbf{x}') \end{aligned} \quad (\text{E21})$$

To leading order in  $N_l$  the averages over  $\mathbf{a}$  and  $\mathbf{W}$  can be performed separately for each layer, and are dominated by their prior, where each element of the weights is an independent Gaussian given by Eq.B5. The term  $m(t, t')$  comes from the covariance of the priors in  $\mathbf{W}$  and  $\mathbf{a}$ , since there are a total of  $L - l$  layers of  $\mathbf{W}$  and one layer of  $\mathbf{a}$ , we have  $m(t, t')^{L-l+1}$ . The kernel  $\dot{\mathcal{K}}^k(t, t', \mathbf{x}, \mathbf{x}')$  comes from the inner product between  $\phi'(z_t^k)$  and  $\phi'(z_{t'}^k)$ , and the kernel  $\mathcal{K}^{l-1}(t, t', \mathbf{x}, \mathbf{x}')$  comes from the inner product between  $\mathbf{x}_t^{l-1}$  and  $\mathbf{x}_{t'}^{l-1}$ .

Using proof by induction as for the NTK [2], we obtain

$$\langle \partial_{\mathbf{w}_t} f(\mathbf{x}, \Theta_t) \cdot \partial_{\mathbf{w}_{t'}} f(\mathbf{x}, \Theta_{t'}) \rangle_0 = e^{T\sigma^{-2}|t-t'|} m(t, t') \dot{\mathcal{K}}^L(t, t', \mathbf{x}, \mathbf{x}') \mathcal{K}^{d, L-1}(t, t', \mathbf{x}, \mathbf{x}') \quad (\text{E22})$$

Combine Eq.E22 with Eq.E19 and with the definition of  $\mathcal{K}_d^L(t, t', \mathbf{x}, \mathbf{x}')$  in Eq.17, we have

$$e^{-T\sigma^{-2}|t-t'|} \langle \nabla_{\Theta_t} f(\mathbf{x}, \Theta_t) \cdot \nabla_{\Theta_{t'}} f(\mathbf{x}', \Theta_{t'}) \rangle_0 = \mathcal{K}_d^L(t, t', \mathbf{x}, \mathbf{x}') \quad (\text{E23})$$

## Appendix F: Representational drift

To capture the phenomenon of representational drift, we consider the case where the learning signal stops at some time  $t_0$ , while the hidden layers continue to drift according to the dynamics of the prior. If all the weights of the system are allowed to drift, the performance of the mean predictor will deteriorate to chance, thus we consider stable readout weights fixed at the end time of learning  $t_0$ . This scenario can be theoretically evaluated using similar techniques to Sec.B, leading to the following equation for the network output:

$$\langle f_{\text{drift}}(\mathbf{x}, t, t_0) \rangle = \int_0^{t_0} (k_d^L(\mathbf{x}, t, t'))^\top (Y - \langle f_{\text{train}}(t') \rangle) \quad (\text{F1})$$

We see here that if  $t_0 = t$  it naturally recovers the full mean predictor. It is interesting to look at the limit where the freeze time  $t_0$  is at NNGP equilibrium. In this case, the expression can be simplified due to the long time identity of the NDK (Eq.16 in the main text).

$$\langle f_{\text{drift}}(\mathbf{x}, t, t_0) \rangle = (k^L(\mathbf{x}, t, t_0))^\top (IT\sigma^{-2} + K_{GP}^L)^{-1} Y \quad (\text{F2})$$

which has a simple meaning of two samples of hidden layer weights from different times at equilibrium. Even at long time differences, the network performance does not decrease to chance, but reaches a new static state.

$$\lim_{t-t_0 \rightarrow \infty} \langle f_{\text{drift}}(\mathbf{x}, t, t_0) \rangle = (k_{\text{mean}}^L(\mathbf{x}))^\top (IT\sigma^{-2} + K_{GP}^L)^{-1} Y \quad (\text{F3})$$

Where the mean kernel is defined in Eq.35. We can evaluate it with the usual kernel functions described in Sec.E, with  $m(t, t_0) = 0, m(t, t) = m(t_0, t_0) = \sigma^2$ .

We can assess the network's ability to separate classes in a binary classification task by using a threshold between the two distributions of outputs, as described in Sec.H.

### 1. Limited Receptive Field

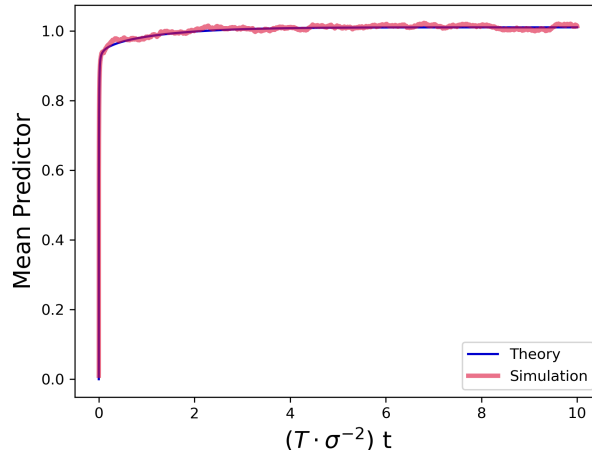
We consider the case where each neuron receives inputs only from a limited patch of the image. The kernel function in this scenario can be calculated by summing up the contribution from each patch:

$$\tilde{\mathcal{K}}(\mathbf{x}, \mathbf{x}') = \sum_{b=1}^B \mathcal{K}(\mathbf{x}_b, \mathbf{x}'_b) \quad (\text{F4})$$

Where the input is split into  $B$  patches, and  $\tilde{\mathcal{K}}$  is the appropriate kernel in this scenario. The predictor can be calculated using the same methods described above with the modified kernel function.

## Appendix G: Theory and Simulation

We compare the predictor calculated using our theory to an ensemble of finite width neural network trained with Langevin learning algorithm (Eq.5) on MNIST binary classification, with the digits 0, 1. We average over 5000 networks to get the mean predictor of the ensemble, and compared it to the theory. The parameters are  $T = 0.01, \sigma = 1, \sigma_0 = 1.44, dt = lr = 0.1$ . The network was trained on  $P = 10$  data points, and its hidden size was  $N = 1000$ . The example presented is the test point 2591 from MNIST test dataset. Theory and simulation show remarkable agreement.



### Appendix H: Details of the numerical simulations

**Figure 1:** We trained 100 deep networks with one hidden layer and an error function nonlinearity using Langevin dynamics (Eq. 5) for binary classification between the 'airplane' and 'frog' categories in the CIFAR-10 dataset [32], with  $P = 400$  data points. The hidden layer size was  $N = 10^4$  neurons, the Langevin dynamics temperature was  $T = 10^{-4}$ , the learning rate  $lr = 0.1$ , the initialization variance  $\sigma_0 = 0.2$ , and the prior variance  $\sigma = 1.0$ . The networks were trained for  $3 \cdot 10^5$  epochs. The test loss in (a) was computed using MSE over 2000 test examples, and the average across all networks is also presented. The training loss in (b) was calculated using MSE over the training set, with the average across all networks also shown. In (c), the dynamics of 100 randomly selected weights from the input to the hidden layer are shown for one network, along with the standard deviation of all the hidden layer weights.

**Figure 2:** The NDK was calculated for MNIST binary classification with the digits 0, 1, for  $P = 100$  data points, and one hidden layer. The NDK was calculated for equal time  $K_d^L(t, t)$  (Eq.15, a-c,g-i), and time difference from initialization  $K_d^L(0, t)$  (Eq.14,d-f,j-l), for ReLU nonlinearity (a-f) and error function nonlinearity (g-l), according to SI Sec.E. For ReLU the parameters are  $\sigma_0 = 0.2, \sigma = 1$ , and for error function  $\sigma_0 = 0.2, \sigma = 10$ .

**Figure 3:** The NTK theory (Sec.V A) was calculated for the ReLU network with one hidden layer, and initialization variance  $\sigma_0 = 1.0$ . The task is binary classification between "airplane" and "frog" in CIFAR-10 dataset with  $P = 200$  data points. The mean predictor, variance, and correlation with the initial condition were calculated according to theory.

**Figure 4:** The covariance in a linear network was calculated according to theory (Eq.29) in a network with one hidden layer and parameters  $\sigma_0 = 1$ . The task is binary classification between "airplane" and "frog" with  $P = 200$  data points. The theory was calculated. In (a), the values of  $\sigma$  are noted in the legend, and in (b),  $\sigma = 1$ .

**Figure 5:** The mean predictor was calculated at the limit  $T \rightarrow 0$ , according to Sec.B 5. The starting point is the NTK equilibrium, after the initial gradient driven phase. The network is with one hidden layer and activation function according to figure titles. The mean field equations at low  $T$  (Eqs.B45, B46) was solved numerically by inverting the  $\{t \times P\} \times \{t \times P\}$  kernel matrix. The theory was calculated with  $dt = 0.0005$ . The task is the binary classification between "airplane" and "frog" in the CIFAR-10 dataset, with  $P = 1000$  data points and  $P_{test} = 2000$  test points. The results presented are the bias averaged over the test points  $\frac{1}{P_{test}} \sum_{\mathbf{x}} (Y(\mathbf{x}) - \langle f(t, \mathbf{x}) \rangle)^2$ . The accuracy was calculated with a threshold at  $\langle f(t, \mathbf{x}) \rangle = 0$ , and the categories label are  $\pm 1$ , such that a correct answer is when the predictor and the label have the same sign.

**Figure 6:** We simulated a deep network with one hidden layer and ReLU neurons. The weights are drawn from a Gaussian distribution with zero mean and variance  $\sigma^2 = 1$ . The hidden layer size is  $N = 10^4$ . For each data point, the hidden layer neuron with maximum activation was chosen, and the activation was normalized by its maximum value such that the diagonal is always 1. (a) The task is binary classification between the digits 0, 1 in MNIST, with  $P = 200$  data points. (b) Binary classification between the digits 4, 9 in MNIST, with  $P = 200$  data points. (c) A low dimensional data was constructed, as a sum of harmonics with decaying amplitude governed by a single scalar  $\theta$ . Each data point  $\mathbf{x}$  obeys  $\mathbf{x} = \sum_{n=1}^{\infty} \frac{1}{n} \mathbf{v}_n \cos(n\theta)$ , where  $\mathbf{v}_n \in \mathbb{R}^N$  is a  $N = 10^4$  dimensional Gaussian vector, which induces both random direction and a random phase.  $P = 200$  angles  $\theta$  were drawn from the range  $[0, \pi]$  such that  $\theta_\mu = \pi\mu/P$ . In the figure, the series was cut at  $n_{max} = 30$ .

**Figure 7:** We simulated a deep network with one hidden layer and ReLU neurons. The weights dynamics

was Langevin dynamics of the Gaussian prior (without learning), such that they obey the time-dependent statistics described in Eq.6, with  $\sigma = 1, T = 10^{-3}$ . The data is the sum of harmonics described in Figure 6 detailed above, and for each data point the neurons with maximum activation was chosen and the activation was normalized. In (a-d) we let each neuron drift according to the prior and track its activation on the different data points, and the times are marked in the title. In (e-h) for each time frame we reorder the same neurons according to their maximum activation, similar to the starting time.

**Figure 8:** We simulated a deep network with one hidden layer and ReLU neurons. The weights dynamics was Langevin dynamics (Eq.5). The network is trained on binary classification in CIFAR-10 dataset between the categories "airplane" and "frog" with  $P = 400$  training data points. The parameters are  $lr = 0.1, \sigma = 0.3, \sigma_0 = 0.7, T = 10^{-3}$ , and the size of the hidden layer is  $N = 10^4$ . The activations of the neurons in the hidden layer were tracked, and for each epoch after  $t_0 = 10^4$ , we computed the SVD of the activation matrix  $\phi(\mathbf{z}_t^{l=1}(\mathbf{x}_\mu)) \in \mathbb{R}^{N \times P}$  for all the training inputs  $\mathbf{x}_\mu$ . For each SVD we took the normalized top right singular vector  $h(\tau) \in \mathbb{R}^P$  and the top left normalized singular vector  $\mathbf{g}(\tau) \in \mathbb{R}^N$ , and computed  $\rho_h(\tau) = h^\top(t_0 + \tau)h(t_0), \rho_g(\tau) = \mathbf{g}^\top(t_0 + \tau)\mathbf{g}(t_0)$ . We plotted the two cosine similarities as a function of time difference from  $t_0$ .

**Figure 9:** We consider the mean predictor with frozen readout weights at time  $t_0$  after learning  $\mathbf{a}(t_0)$ , and the hidden layers weights  $\mathbf{W}(t)$  drift without learning. We calculate the mean predictor in this scenario using Eq.34, in MNIST dataset with  $P = 10^4$  training data points. For each time  $t$  (in the titles of the subfigures), we trained a threshold  $C$  using perceptron algorithm such that  $f > C$  is classified as +1 and  $f < C$  is -1, and the target labels are the original labels of the data points. The accuracy was evaluated by comparing the classification of the threshold and the original labels.

**Figure 10:** We consider the mean predictor with frozen readout weights at time  $t_0$  after learning  $\mathbf{a}(t_0)$ , and the hidden layers weights  $\mathbf{W}(t)$  drift without learning, in MNIST dataset with  $P = 2 \cdot 10^4$  training data points. Each neuron receives inputs from a limited receptive field. To simulate that, we split each MNIST image to  $B^2$  patches, where each patch is with size  $m \times m$ , and  $B = 28/m$ . We calculate the mean predictor in this scenario using Eq.34, with a modified kernel as described in SI Sec.F 1. Similar methods to Figure 9 were used to asses the accuracy in this scenario.